Research Square

Preprints are preliminary reports that have not undergone peer review.
They should not be considered conclusive, used to inform clinical practice,
or referenced by the media as validated information.

Earthquake-Induced Liquefaction Potential and Post-Liquefaction Settlement Analysis for Coastal Infrastructure Development on Moheshkhali Island, Bangladesh

Omar Faruk
University of Dhaka
Mohammad Feruj Alam
Geological Survey of Bangladesh
Md. Mostafizur Rahman
University of Dhaka
Mohammad Solaiman
University of Dhaka
Md. Anwar Hossain Bhuiyan
ahb@du.ac.bd

University of Dhaka

Research Article

Keywords: Earthquake, Factor of Safety, Liquefaction Potential Index, Settlement, Coastal Infrastructure Development, Moheshkhali Island

Posted Date: November 12th, 2026

DOI: https://doi.org/10.21203/rs.3.rs-11531947/v1

License: This work is licensed under a Creative Commons Attribution 4.0 International License.
Read Full License

Additional Declarations: No competing interests reported.

Earthquake-Induced Liquefaction Potential and Post-Liquefaction Settlement Analysis for Coastal Infrastructure Development on Moheshkhali Island, Bangladesh

Abstract

Purpose: Earthquake-induced liquefaction and associated ground settlement threaten coastal infrastructure, yet Moheshkhali Island, Bangladesh, lacks a site-specific liquefaction hazard assessment despite active seismicity and planned infrastructure development. This study investigates the spatial variability of liquefaction potential and what this implies for resilient coastal infrastructure development.

Methods: Borehole SPT data were used for liquefaction triggering analysis, the Liquefaction Potential Index (LPI), and post-liquefaction ground settlement estimation under three earthquake magnitude sensitivity scenarios (M_w = 5.2, 6.0, and 7.0) with a common code-based PGA of 0.28 g, and fine-grained soil susceptibility assessment.

Results: Subsurface conditions were heterogeneous, producing spatial and depth-wise variability in liquefaction response controlled by soil density, fines content, stratigraphy, groundwater depth, and seismic loading. Saturated loose-to-medium-dense sandy soils are highly susceptible to liquefaction, whereas fine-grained soils exhibit variable susceptibility depending on moisture content and plasticity. BH-02 shows the highest LPI values in all cases (5.75, 18.72, and 29.59) and the highest estimated free-field settlement at M_w 7.0 (28.87 cm), identifying it as the most liquefaction-potential site. Site rankings differed among LPI, settlement, and surface manifestation potential. A relatively dense, non-liquefiable silty sand layer (N > 30) persisted under all scenarios.

Conclusion: No single indicator adequately captures damage potential in these interlayered deposits. The dense silty sand layer may provide a suitable bearing stratum for deep foundations. Because liquefaction response varies over short distances, site-specific assessment is essential, and these findings offer practical guidance for resilient and sustainable coastal infrastructure development in similar heterogeneous subsurface conditions.

Keywords: Earthquake, Factor of Safety, Liquefaction Potential Index, Settlement, Coastal Infrastructure Development, Moheshkhali Island.

1 Introduction

Earthquake-induced soil liquefaction is one of the most severe secondary seismic hazards and is responsible for catastrophic ground failure, lateral spread, and foundation instability globally [1–3]. When saturated, cohesionless and low-plasticity soils experience cyclic shaking during earthquake ground motion, excess pore pressure increases, and the effective stress decreases, potentially causing liquefaction and abrupt loss of shear strength and bearing capacity [1, 4]. Historically, earthquake-induced liquefaction, namely the Nobi Earthquake of 1891, the Tonankai Earthquake of 1944, the Niigata and Alaska earthquakes of 1964, and the Loma Prieta earthquake of 1989, have demonstrated the destructive capacity of this phenomenon by causing structural damage, casualties, and significant economic loss [5, 6]. Therefore, assessing the liquefaction risk of saturated loose soils in earthquake-prone areas for sustainable infrastructure and site characterization is necessary to mitigate geotechnical risk [7, 8].

The foundational framework for deterministic liquefaction assessment was introduced by Seed and Idriss [1] known as simplified procedure. The simplified procedure calculates the factor of safety (F.S.) against liquefaction by comparing the cyclic stress ratio (CSR) to the soil's intrinsic cyclic resistance ratio (CRR). Over the past several decades, this procedure has been continuously calibrated and expanded via extensive field performance data from sites that did and did not liquefy during major earthquakes [5, 9–12]. In situ tests have become widely popular because collecting undisturbed soil samples from loose, saturated sandy and silty layers is both difficult and expensive [7]. Among in-situ methods, the Standard Penetration Test (SPT) remains the most widely adopted method due to its extensive historical performance database and ability to retrieve disturbed samples for fines content analysis [12, 13]. Several researchers have conducted research for liquefaction assessment using the SPT-based simplified procedure [7, 14–18]. Although the factor of safety indicates whether a soil layer is resistant to liquefaction, it provides an incomplete assessment of overall surface manifestations and structural damage potential [8, 19]. Consequently, it is not a sufficient standalone parameter to assess the true severity of liquefaction [20]. To address this problem, Iwasaki et al. [5, 21] developed the Liquefaction Potential Index (LPI) by incorporating the factor-of-safety values, the thickness of each liquefiable layer, and their proximity to the ground surface (typically up to 20 m depth). This method has been used by researchers for liquefaction hazard mapping both in Bangladesh and around the world [2, 8, 19, 22–25].

Post-liquefaction settlement, caused by the dissipation of excess pore water pressure, represents a secondary but critically important consequence of liquefaction triggering. Tokimatsu and Seed [26] established that volumetric strain is governed primarily by the maximum cyclic shear strain developed during shaking and the relative density of the soil. Ishihara and Yoshimine [4] further refined this approach by directly linking post-liquefaction volumetric strains to the factor of safety against liquefaction. The Ishihara and Yoshimine [4] methodology is widely used for post-liquefaction settlement calculation [2, 27].

Moheshkhali Island, situated along the southeastern coast of Bangladesh within the active Chittagong-Tripura Fold Belt (CTFB), occupies a critically complex geotectonic setting near the active Indo-Burman subduction margin [28]. The presence of the Kaladan Fault and the Chittagong Coastal Fault increases its vulnerability to seismic hazards [29]. There is also evidence of a 5.2 magnitude earthquake on July 22, 1999, at a focal depth of 10 km [30]. According to the BNBC [31] seismic zoning map, this island is designated Zone III, with a peak ground acceleration (PGA) of 0.28 g, classifying it as a seismically active, high-hazard zone. The island is also

characterized by unconsolidated heterogeneous Holocene coastal deposits comprising alternating sandy and fine-grained strata, reflecting spatial variation in depositional conditions [32]. Previous studies have indicated the high liquefaction potential of Holocene sandy and silty soils [3, 7]. Despite the documented seismic activity in proximity to the active Indo–Burman subduction zone and the presence of Holocene loose soil deposits, no comprehensive liquefaction hazard assessment has been performed on Moheshkhali Island. The necessity of addressing this gap is amplified by the mid-term development plan, proposed by the Government of Bangladesh in Moheshkhali Upazila with 17 infrastructure projects, including power plants, gas pipelines, liquefied natural gas (LNG) import terminals, and special industrial economic zones [33]. The failure of such infrastructure due to liquefaction-induced settlement or ground instability could have consequences far exceeding those of ordinary building damage.

Previous coastal studies have generally treated triggering, hazard mapping and settlement separately or in partial combination, with varying treatment of fine-grained soils. Yilmaz and Yavuzer [23] mapped the susceptibility and liquefaction potential of the coastal city of Turkey, and Al-Enezi et al. [22] conducted research using liquefaction potential index with varying earthquake scenarios on coastal cities of Kuwait. On the other hand, Misliniyati et al. [17] calculated the factor of safety, probability of liquefaction, and post-liquefaction ground settlement for the Bengkulu port area in Indonesia while skipping liquefaction potential analysis despite it being a highly seismic region. Cho et al. [18] and Seo et al. [16] have assessed the liquefaction susceptibility of fine-grained soils of coastal areas of Korea using the Bray and Sancio [34] criteria. Several studies have been conducted on Holocene coastal deposits in Bangladesh using factor of safety and liquefaction potential index [2, 7, 24]. Mahabub et al. [27] and Hossain et al. [2] have combined triggering, hazard severity, and post-liquefaction but did not evaluate the susceptibility of fine-grained soils. Field evidence suggests that relying on single indicator can fail: LPI categories do not always agree with observed manifestation [35], and the thickness of the non-liquefied crust controls whether liquefaction reaches the surface [36]. This contrast should be strongest in interlayered sand–silt–clay sequences, such as the Holocene coastal deposits of Moheshkhali Island [37]. Whether, and why, the common indicators rank sites differently in such deposits has not been examined for Bangladesh, and the practical consequence, that a hazard class based on one indicator may misrepresent damage potential, has not been demonstrated at a site where major infrastructure is planned. The influences of lithological heterogeneity and depositional variability on the combined liquefaction response and settlement behavior of the Holocene coastal deposits also remain insufficiently understood, especially for Bangladesh. But for critical infrastructure development combined assessment is necessary for such complex geological and heterogenous setting.

This study addresses these gaps by introducing a site-specific liquefaction hazard assessment of Moheshkhali Island, combining: i) site-specific liquefaction triggering analysis using the deterministic method of Seed and Idriss [1]; ii) liquefaction potential using the Liquefaction Potential Index (LPI) proposed by Iwasaki et al. [21]; iii) post-liquefaction settlement estimation using the method of Ishihara and Yoshimine [4] using the LiquefyPro software; and iv) liquefaction susceptibility assessment of fine-grained soil using the plasticity-based criteria of Bray and Sancio [34]. These analyses are evaluated across three deterministic earthquake magnitude scenarios (M_w = 5.2, 6.0, and 7.0) with a common code-based peak ground acceleration (PGA) of 0.28 g, as magnitude sensitivity study, to examine how increasing earthquake magnitude affects liquefaction triggering, liquefaction potential, and ground settlement. This study also aims to identify how geological and geotechnical factors, along

with stratigraphic heterogeneity, influence triggering and earthquake-induced ground deformation. This integrated evaluation of liquefaction triggering, liquefaction severity, post-liquefaction settlement, and the behavior of fine-grained soils can provide a broader basis for understanding how stratigraphic heterogeneity influences liquefaction potential. Furthermore, this study delineates a competent non-liquefiable sandy layer that may represent a potentially favorable founding zone for deep foundations. Ultimately, this study provides preliminary guidance for planning further investigation at proposed coastal infrastructure sites on Moheshkhali Island, while offering an analytical framework for liquefaction hazard assessment in analogous complex Holocene coastal environments.

2 Geomorphology and Geology of the Study Area

Moheshkhali Island, situated in the southeastern part of Bangladesh, is the only hilly island in the country (Fig. 1). It is separated from the Cox's Bazar mainland by the Moheshkhali Channel [38]. The island is bounded by Pekua Upazila to the north, Chakaria Upazila to the northeast, and Cox's Bazar Sadar to the southeast, whereas its western and southern margins are exposed to the Bay of Bengal. Moheshkhali Island represents a complex geological system on the eastern coast of Bangladesh. The island is characterized by hilly terrain surrounded by coastal plains and has unique geological, tectonic, and geomorphological characteristics [39]. The hilly terrain reaches elevations of up to 63 m above mean sea level. The island is also subjected to strong tidal currents, cyclonic storm surges, and shoreline shifts associated with the Bay of Bengal, which influence the landscape, sediment distribution, and groundwater conditions [38]. The southwestern and western coastal plains of Moheshkhali Island have undergone significant land accretion through sediment deposition, contributing to the expansion of the island's landmass at an average rate of approximately 1.2 km² per year since 1972 [39]. Sediments from hills, consisting mostly of sand and silty clay, are deposited in coastal plains [32].

The broader landscape can be divided into distinct physiographic units, including a hilly area surrounded by piedmont plains, an old coastal plain, a young coastal plain, and an active coastal plain. Notable geomorphic units are as follows:1. Tertiary hill deposits, 2. Supratidal deposits, 3. Intertidal deposits, 4. Piedmont deposits, 5. Barrier beach deposits, 6. Dune deposits, and 7. Paleo-beach deposits [32]. Tectonically, the island lies within the folded flank Tectonic element and is characterized by sub-meridional structural trends developed within Neogene sediments [32]. The hills of the island constitute the Moheshkhali Anticline, whose axis runs north-northwest to south-southeast (NNW-SSE) and plunges north-northwest [30]. The axial trend of this structure is curvilinear in its central segment and exhibits an en-echelon relationship with the axial trends of the neighboring anticlines. The hills of Moheshkhali are composed of Surma Group, Tipam, Girujan, and Dupitila formations of Tertiary age and Dihing Formation of Quaternary age [32, 38]. Figure 1 shows the study area location.

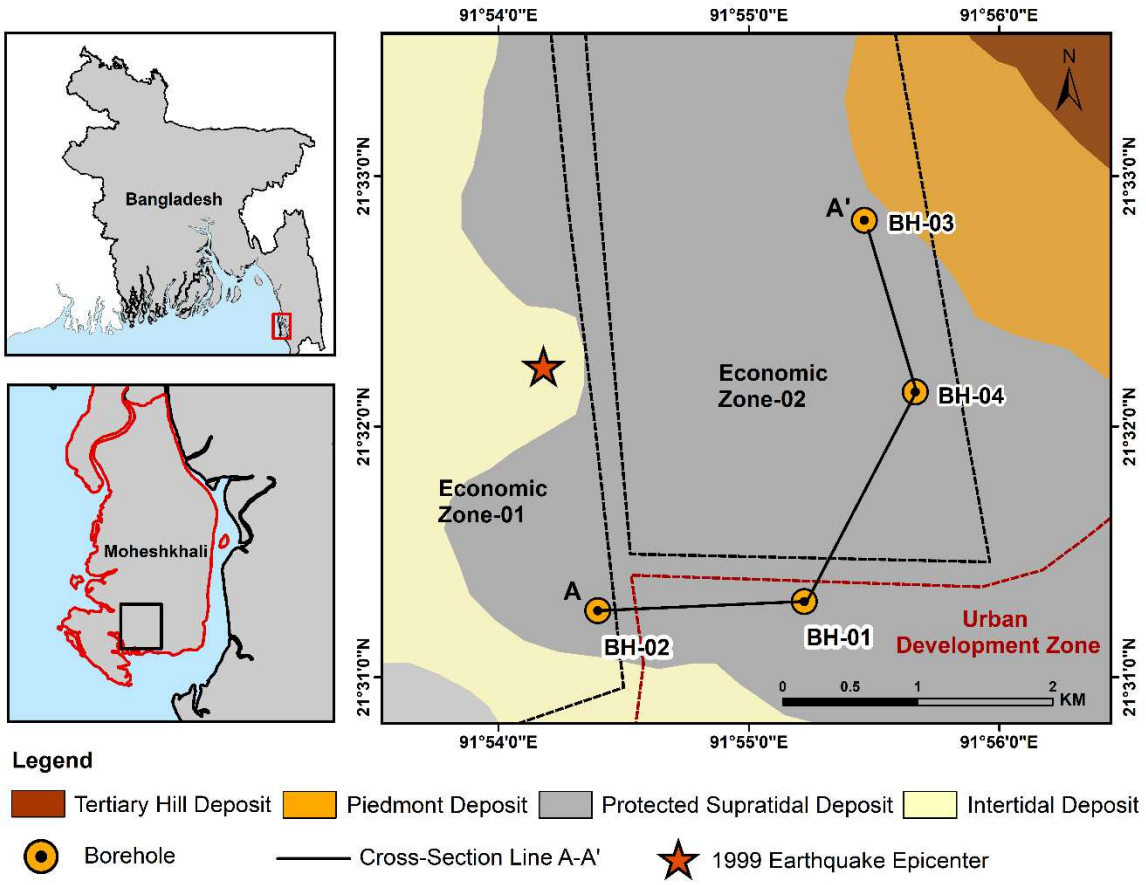

Fig. 1 Surface geological map of the study area and borehole locations in the protected supratidal deposits (modified after Majlis et al. [32])

3 Seismotectonics

The Bengal Basin is surrounded by the Shillong Plateau to the north, the Precambrian Indian Shield to the west, the Indo-Burman Range (IBR) to the east, and the Bay of Bengal to the south [40]. It is a complex foreland basin south of the Himalayas, with a thick sediment pile (22 km) of Early Cretaceous–Holocene age, reflecting complex depositional and tectonic development [41]. This basin is located at the juncture of three active plates, namely the Indian plate, the Eurasian plate, and the Burmese plate, making it a dynamic and tectonically active region [28]. Several large earthquakes have occurred in and around the area due to active plate boundaries and faults, making it a seismically active region [19, 42]. The Bengal-Arakan earthquake of 1762, the Cachar earthquake of 1869, the Bengal earthquake of 1885, the Great Indian Earthquake of 1897, and the Srimangal earthquake of 1918 caused significant damage in this basin [29].

Bangladesh lies in the central part of the Bengal Basin, covering almost three-quarters of the basin [43]. The Indo-Burman Range, located east of Bangladesh, marks the active subduction zone where the Indian Oceanic Plate is subducting beneath the Burmese continental plate, with the two plates meeting at a locked megathrust boundary [42, 44]. Subduction and highly oblique convergence of the Indo-Burman Range (IBR) have created a complex network of thrust faults and dextral faults [44, 45]. Several major faults are present within the Indo-Burmese plate

boundary zone, including the Kaladan Fault, Churachandpur Fault, Kabaw Fault, and Naga Thrust Fault [29, 45] (Figure 2).

The study area lies in the Chittagong-Tripura Fold Belt (CTFB), which is an active accretionary wedge and the westernmost part of the IBR, consisting of a series of north-south trending curvilinear anticlines and synclines [43]. It is separated from the central foredeep and eastern IBR by two active faults, which are the Chittagong Coastal Fault (CCF) to the west and the dextral Kaladan Fault to the east [28]. Clustering of major earthquakes and recent seismicity around the CCF and Kaladan fault indicate that the blocks are still active [42, 45]. Moheshkhali Island experienced a 5.2-magnitude earthquake on July 22, 1999, with a focal depth of 10 km at 21.544°N and 91.895°E, and the intensity of the earthquake was VII 'damaging type' on the EMS scale [30].

BNBC [31] divides Bangladesh into four seismic zones on the basis of maximum considered peak ground acceleration (PGA) values shown in Figure 3. The zones are Zone I, Zone II, Zone III, and Zone IV, having PGA values of 0.12 g, 0.20 g, 0.28 g, and 0.36 g, respectively. Moheshkhali Island is located in Zone III and has a PGA value of 0.28 g, indicating an intensive zone. Moreover, fractures are observed along the Moheshkhali Anticline, which indicates that the shallow imbricate local thrust system beneath the island remains tectonically active and has the potential to generate moderate earthquakes [29, 42, 45].

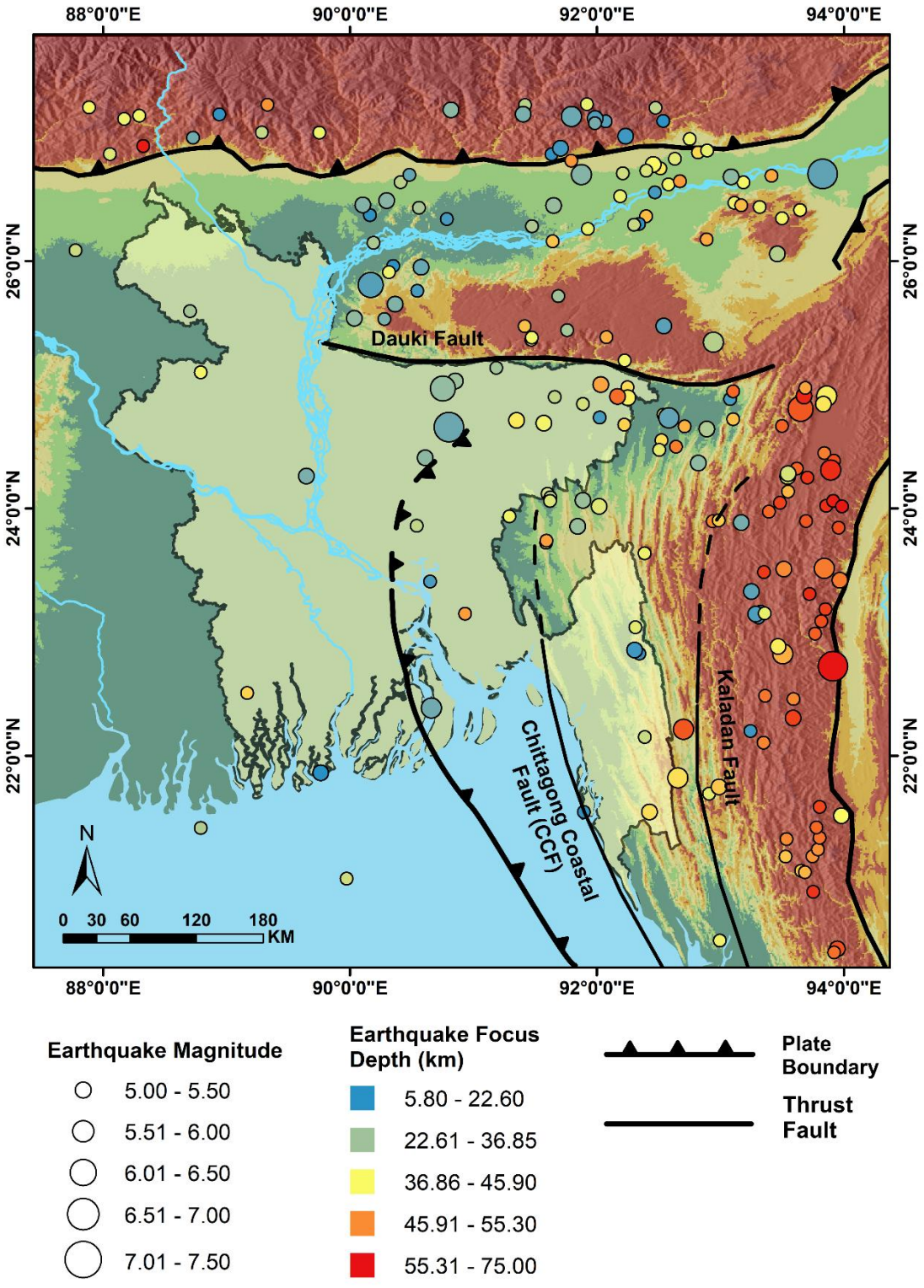

Fig. 2 Seismotectonic map of Bangladesh and nearby regions showing earthquake epicenters from 1900 to 2025 with magnitudes of 5 and greater. The color code shows the depth range of hypocenters, and earthquake magnitudes are shown using proportional symbols that increase with magnitude. The plate boundaries and faults are from Steckler et al. [44] and Hossain et al. [29].

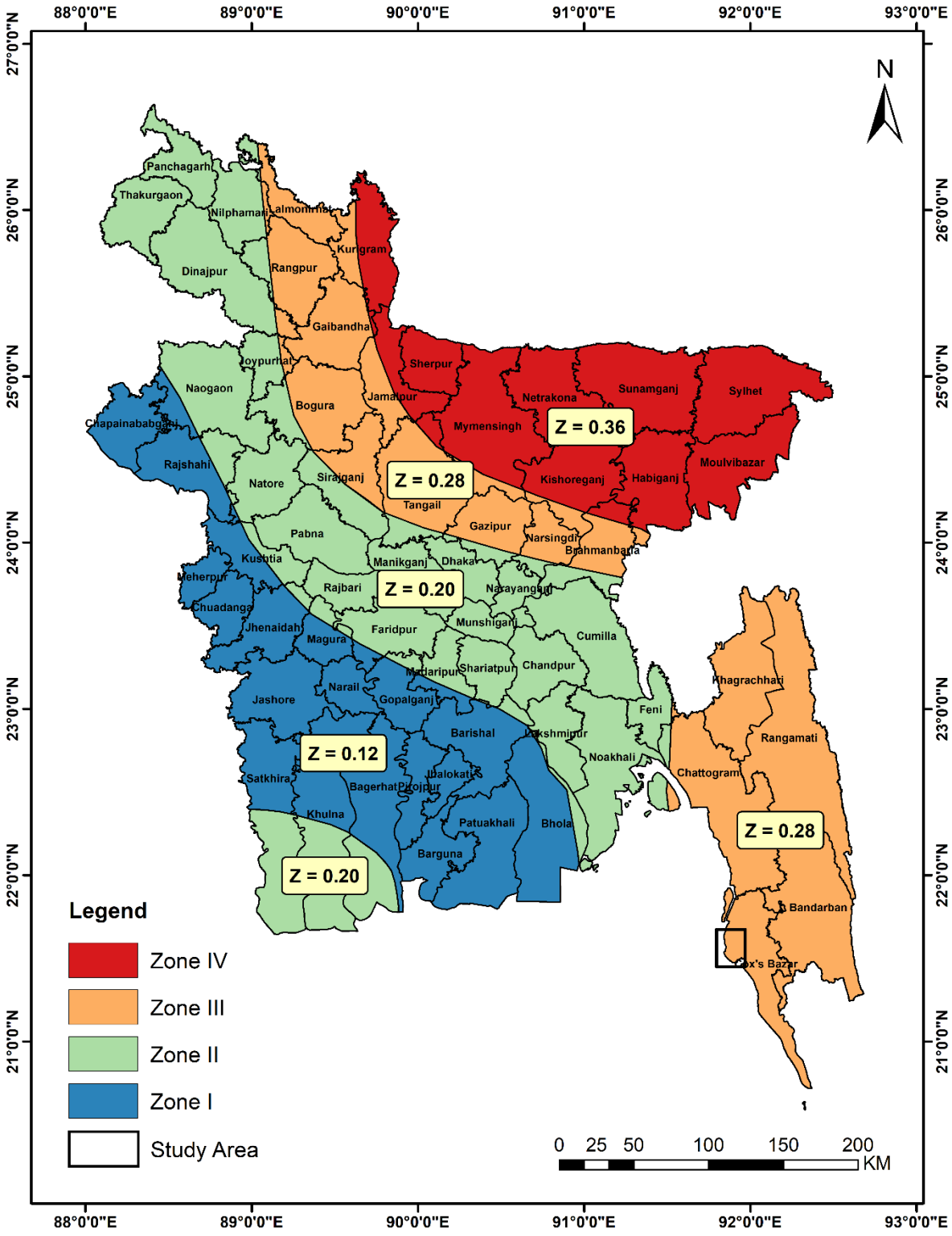

Fig. 3 Seismic zonation map of Bangladesh showing peak ground acceleration (PGA) values [31]. The black box indicates the location of the study area which falls within Zone III (PGA = 0.28 g)

4 Materials and Methods

This research is divided into two major stages: i) field and laboratory geotechnical investigations for subsurface characterization, and, ii) liquefaction hazard assessment using the resulting dataset. LiquefyPro [46] software was used to calculate the factor of safety (F.S.) and the post-liquefaction settlement of the soil layers. The liquefaction potential index (LPI) was calculated from the resulting factor-of-safety values. Two-dimensional cross-sections and lithologies were produced using RockWorks 16 software.

4.1 Geotechnical Investigation

Subsurface characterization of the study area includes both in-situ testing and laboratory analyses. Four boreholes were drilled using the Standard Penetration Test (SPT) technique in accordance with ASTM D1586. Soil sampling was performed at 1.5 m intervals using split-spoon sampler, and the collected samples were subjected to further laboratory analysis. The decision to select the locations of boreholes is based on the Government's infrastructure development plans and their proximity to the 1999 earthquake epicenter. The borehole locations within the protected supratidal surface geological unit are shown in Figure 1. Data up to a depth of 19.5 m were used for liquefaction potential analysis, which is a standard practice for liquefaction assessment [21]. A comprehensive suite of index geotechnical tests including natural moisture content (ASTM D2216), specific gravity (ASTM D854), grain size analysis by mechanical sieve and hydrometer methods (ASTM D6913 and D7928, respectively) and Atterberg limit tests (ASTM D4318) were performed on the collected samples. All tests were conducted in accordance with the relevant ASTM standards. The soils were further classified according to the Unified Soil Classification System (USCS), as specified in ASTM D2487, on the basis of laboratory test results. The depth to the groundwater table was measured at all four boreholes 24 hours after drilling was completed to allow stabilization of the groundwater level. The recorded depths were used for liquefaction potential analysis in this study. The measured depth should therefore be regarded as a representative field observation rather than a continuous measurement.

4.2 Liquefaction Hazard Assessment

The liquefaction hazard assessment was done by assessing the susceptibility of fine-grained soils and the widely adopted SPT-based simplified procedure, incorporating three complementary analytical components: i) liquefaction triggering evaluation, ii) liquefaction potential indexing, and iii) post-liquefaction settlement quantification.

4.2.1 Liquefaction Susceptibility of Fine-Grained Soil

In general, cohesionless sandy soils are highly vulnerable to liquefaction, whereas the majority of fine-grained soils (cohesive soils) are not susceptible to liquefaction [10]. The liquefaction susceptibility of fine-grained soils is commonly evaluated using the Chinese criteria [12]. Bray et al. [47] reported that many fine-grained soils classified as non-liquefiable under the Chinese criteria [10, 12] have been found to liquefy during recent earthquakes. The liquefaction susceptibility of fine-grained soils is better represented by the amount and type of clay minerals than by the clay-sized particle content alone [34, 47]. Bray and Sancio [34] conducted cyclic laboratory testing on fine-grained soil samples from previous earthquake sites and proposed a new criterion. This approach relates the plasticity index (PI) and the natural water content to the liquid limit ratio (W_c/LL). According to Bray and Sancio [34], soils with PI < 12 and W_c/LL > 0.85 are generally susceptible to liquefaction, whereas soils with 12 ≤ PI ≤ 18 and W_c/LL > 0.80 are moderately susceptible, and soils with PI > 18 are generally not

susceptible. This criterion was applied to all the fine-grained samples in the present study for assessing the liquefaction susceptibility.

4.2.2 Liquefaction Triggering Analysis: Factor of Safety (F.S.) Calculation

Liquefaction resistance of soil can be evaluated by factor of safety values using the simplified procedure proposed by Seed and Idriss [1], which was later modified and improved by several scientists and implemented in the software used in this study. This deterministic approach allows assessment of liquefaction resistance using a factor of safety at specific depths where SPT N-values are available. A soil layer is considered liquefiable when F.S. < 1.0, whereas it is considered non-liquefiable when F.S. > 1.0 [31]. The value of the factor of safety mainly depends on two parameters: i) seismic loading on the soil, represented by the Cyclic Stress Ratio (CSR), and ii) the resistance of the in-situ soil to liquefaction under seismic loading, represented by the Cyclic Resistance Ratio (CRR) [12].

The Cyclic Stress Ratio (CSR) was calculated using the following equation proposed by Seed and Idriss [1]:

$$\mathrm{CSR} = 0.65\left(\frac{\sigma_o}{\sigma_o'}\right)\left(\frac{a_{max}}{g}\right)r_d \quad (1)$$

Where, σ_o= total vertical stress, σ'_o = effective vertical stress, a_{max} = peak ground acceleration, and g = acceleration of gravity.

The stress reduction coefficient, $r_{d,}$ is dependent on the depth of the soil layer (z) below the ground surface, which was determined by using the following equation of Liao and Whitman [48]:

$$r_d = 1.0 - 0.00765 * z \quad \text{for } z \leq 9.15\ \text{m} \quad (2.a)$$

$$r_d = 1.174 - 0.0267 * z \quad \text{for } 9.15 < z \leq 23\ \text{m} \quad (2.b)$$

Another important parameter of the simplified procedure is the Cyclic Resistance Ratio (CRR), which represents the resistance of the soil to liquefaction and indicates the soil strength. It was calculated by the following empirical formula, which is implemented in the software [49]:

$$\mathrm{CRR}_{7.5} = \frac{0.048 - 0.004721x + 0.0006136x^2 - 0.00001673x^3}{1 - 0.1248x + 0.009578x^2 - 0.0003285x^3 + 0.000003714x^4} \quad (3)$$

Here, x represents the value of $(N_1)_{60cs}$.

$(N_1)_{60cs}$ represents the corrected SPT N-value (Clean sand equivalent), which is normalized to an overburden pressure of 100 kPa and the fine content effect [12]:

$$(N_1)_{60cs} = \alpha + \beta(N_1)_{60} \quad (4)$$

$$\alpha = 0, \beta = 1 \text{ for FC} \leq 5\% \quad (5.a)$$

$$\alpha = \exp\left[1.76 - \left(\frac{190}{FC^2}\right)\right], \beta = \left[0.99 + \left(\frac{FC^{1.5}}{1000}\right)\right] \text{ for } 5\% < FC < 35\% \quad (5.b)$$

$$\alpha = 5, \beta = 1.2 \text{ for FC} \geq 35\% \quad (5.c)$$

Where, FC is the fine content (%) and α and β are correction coefficients used to account for the influence of fine content.

The term $(N_1)_{60}$ is used to denote the corrected SPT N-value for field procedures when the hammer energy ratio is 60% and normalized for effective overburden pressure. It is calculated using the given equation [50]:

$$(N_1)_{60} = N_m C_n C_e C_b C_r C_s \quad (6)$$

Where, N_m is the raw SPT N-value, C_n is the normalized effective overburden correction factor, C_e is the hammer energy ratio correction factor, C_b is the correction factor for borehole diameter, C_r is the rod length correction factor, and C_s = sampler correction factor. The following values were used as input parameters in the software:

C_e = 0.6 for donut hammer, C_b = 1.0 for borehole diameter of 65-115 mm, C_s = 1.0 for standard sampler and C_r = 0.75 for 1 to 3 m, 0.80 for 3 to 4 m, 0.85 for 4 to 6 m, 0.95 for 6 to 10 m, and 1.0 for > 10 m rod length.

The overburden stress correction factor, C_n can be expressed by the following equation [48]:

$$C_n = \left(\frac{P_a}{\sigma_0'}\right)^{0.5} \quad (7)$$

Where, P_a is the atmospheric pressure of 100 kPa, σ_0' is the effective vertical overburden stress, and C_n is limited to a maximum value of 1.7.

According to Youd et al. [12] the factor of safety is calculated from the Cyclic Stress Ratio (CSR), Cyclic Resistance Ratio (CRR), and Magnitude Scaling Factor (MSF), which is expressed as follows:

$$FS_L = \frac{CRR_{7.5} MSF}{CSR} \quad (8)$$

The MSF is used to account for the effects of earthquake magnitudes different from 7.5 because the $CRR_{7.5}$ is calculated based on a 7.5 magnitude earthquake. For any earthquake less than or greater than 7.5 magnitude it needs to be corrected using the following equation [12]:

$$MSF = \frac{10^{2.24}}{M_w{}^{2.56}} \quad (9)$$

Where, M_w is the earthquake magnitude used for calculation other than 7.5 magnitude.

4.2.3 Liquefaction Potential Index (LPI)

The severity of liquefaction cannot be estimated solely from the factor of safety values, as it only indicates whether a soil layer is likely to liquefy under seismic loading [20]. Therefore, the severity of liquefaction can be mapped by using the Liquefaction Potential Index (LPI) [19, 24]. To assess the liquefaction potential of an area, Iwasaki et al. [5, 21] proposed Liquefaction Potential Index (LPI) by considering the depth and thickness of liquefiable layers along with the factor of safety values. The index is expressed as:

$$P_L = \int_0^{20} F(z)\, W(z) dz \quad (10)$$

$$F(z) = 1 - F.S. \text{ for } F.S. < 1.0 \quad (11.a)$$

$$F(z) = 0 \text{ for } F.S. \geq 1.0 \quad (11.b)$$

$$W(z) = 10 - 0.5z \text{ for } z < 20m \quad (11.c)$$

$$W(z) = 0 \text{ for } z > 20m \quad (11.d)$$

Where, z denotes the soil layer depth measured from the ground surface in meters. $F(z)$ is the liquefaction severity factor, and $W(z)$ is the depth weighting factor. The liquefaction potential can be assessed by using the classification of Iwasaki et al. [21] (Table 1).

Table 1 LPI-based risk classification proposed by Iwasaki et al. [21]

LPI	Liquefaction potentiality
0	Very Low
0 < LPI ≤ 5	Low
5 < LPI ≤ 15	High
LPI > 15	Very High

4.2.4 Post-Liquefaction Settlement Quantification

Saturated soil tends to settle when the earthquake-induced excess pore water pressure dissipates, resulting in post-liquefaction ground settlement [26]. In this study, settlement analysis was performed for the liquefied soils using the method proposed by Ishihara and Yoshimine [4], as implemented in LiquefyPro software. In this method, the volumetric strain ($\in_v$) of a liquefied layer is primarily affected by the relative density (D_r), estimated from $(N_1)_{60}$, and maximum shear strain, which is directly related to the factor of safety ($F.S.$). The software calculates the volumetric strain from the curves provided by Ishihara and Yoshimine [4], which show the relationship between the post-liquefaction volumetric strain and the factor of safety. The settlement induced in each soil layer is estimated by multiplying the volumetric strain by the thickness of each layer by the following equation:

$$S_{sat} = \left(\frac{\in_v}{100}\right) dz \tag{12}$$

Where, S_{sat} represents the settlement of the saturated soil layer, $\in_v$ is the volumetric strain (%), and dz represents the soil layer thickness. Settlement was computed only for layers with F.S. < 1.0. Finally, the post-liquefaction total settlement (S_{Total}) at the ground surface is calculated by the following equation:

$$S_{Total} = \sum_{i=1}^{n} \in_{vi} dz \tag{13}$$

4.2.5 Seismic Factors

Two ground motion parameters are essential for liquefaction resistance assessment of soil using the simplified procedure: i) peak horizontal ground acceleration and ii) magnitude of earthquake [12]. In this study, liquefaction hazard assessment was performed under three earthquake scenarios with magnitudes of 5.2, 6.0, and 7.0, using a peak horizontal ground acceleration of 0.28 g, corresponding to the study area's location in Seismic Zone III according to the BNBC [31] seismic zonation map. A common PGA was adopted to examine the sensitivity of the liquefaction response to earthquake magnitude rather than to reconstruct event-specific ground motions. The 5.2 earthquake magnitude was selected for previously documented 1999 earthquake event, with the epicenter close to the investigated borehole sites, but the acceleration of that event was not reconstructed. The magnitude 6.0 and 7.0 scenarios were selected to represent progressively stronger seismic conditions. The reported results should be interpreted as conditional magnitude-sensitivity estimates rather than a complete seismic-hazard assessment or a substitute for site-specific design ground motions.

5 Results

5.1 Geotechnical Characteristics

The collected soil samples from the four boreholes were tested in the laboratory to determine the index geotechnical properties and classify the soil. The subsurface stratigraphy across all boreholes consists of alternating layers of poorly graded sand (SP), poorly graded sand with silt (SP-SM), silty sand (SM), silt (ML), lean clay (CL), and fat clay (CH) (Figure 4). The SPT N values range from 6 to 60 across the boreholes, indicating variable density in subsurface layers. The grain-size distribution analysis indicates that most of the soil samples are coarse-grained. The grading properties of soil, such as the uniformity coefficient (C_u), range from 1.77 to 5.37, and the coefficient of curvature (C_c) ranges from 0.52 to 1.50. The values indicate poorly graded and well-sorted sandy soils as it follows the USCS classification criteria where $C_u < 6.0$ and/or $C_c < 1.0$ or $C_c > 3.0$ and finally classified as SP, SP-SM, or SM depending on fine content and nature of the fines. The thickness and alternation

of these layers also vary across the island. Moreover, most of the cohesionless soils fall within the highly susceptible region of the gradation-based liquefaction susceptibility curves proposed by Iwasaki [51] for uniformly graded soils (Figure 5). The fine-grained soils are classified using the Atterberg limit test results and classified as CH, ML, and CL. The Liquid Limit (LL) values range from 23.39% to 51.43%, the Plastic Limit (PL) values range from 13.97% to 25.55%, and the Plasticity Index (PI) values range from 8.33% to 25.92% (Table 3). BH-01 and BH-02 are primarily composed of poorly graded sand with silt and silty sand containing non-plastic fines. Fluctuations in SPT N-values within the upper 10 m were observed in BH-02, whereas a consistently dense layer was identified below 4.5 m in BH-01. Below 18 m depth, a lean clay (CL) layer with varying plasticity characteristics is observed in both boreholes. In BH-03, an intermediate clay-rich layer occurs between depths of approximately 13.5 and 15.0 m depth and is characterized by relatively high liquid limit and plasticity index values. BH-04 contains a comparatively thicker sandy lean clay (CL) layer between depths of 12 and 15 m depth, with liquid limit values ranging from 23.39% to 26.86%. A zone of high penetration resistance (N > 30) is observed across all boreholes at varying depths, indicating the presence of dense sandy deposits, consisting of silty sand (SM).

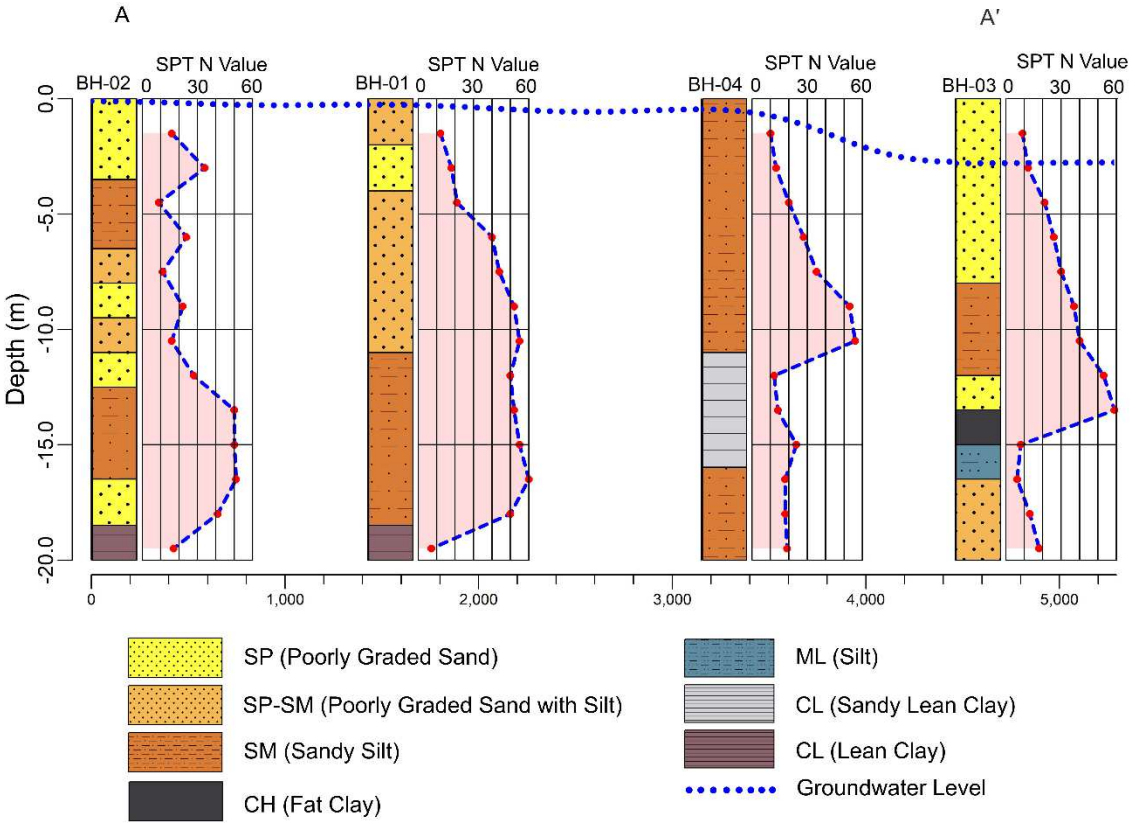

Fig. 4 Subsurface soil profiles of all four boreholes based on the Unified Soil Classification System (USCS), with corresponding SPT N-values plotted against depth. The blue dotted line represents the groundwater table depth along the A–A′ cross-section line

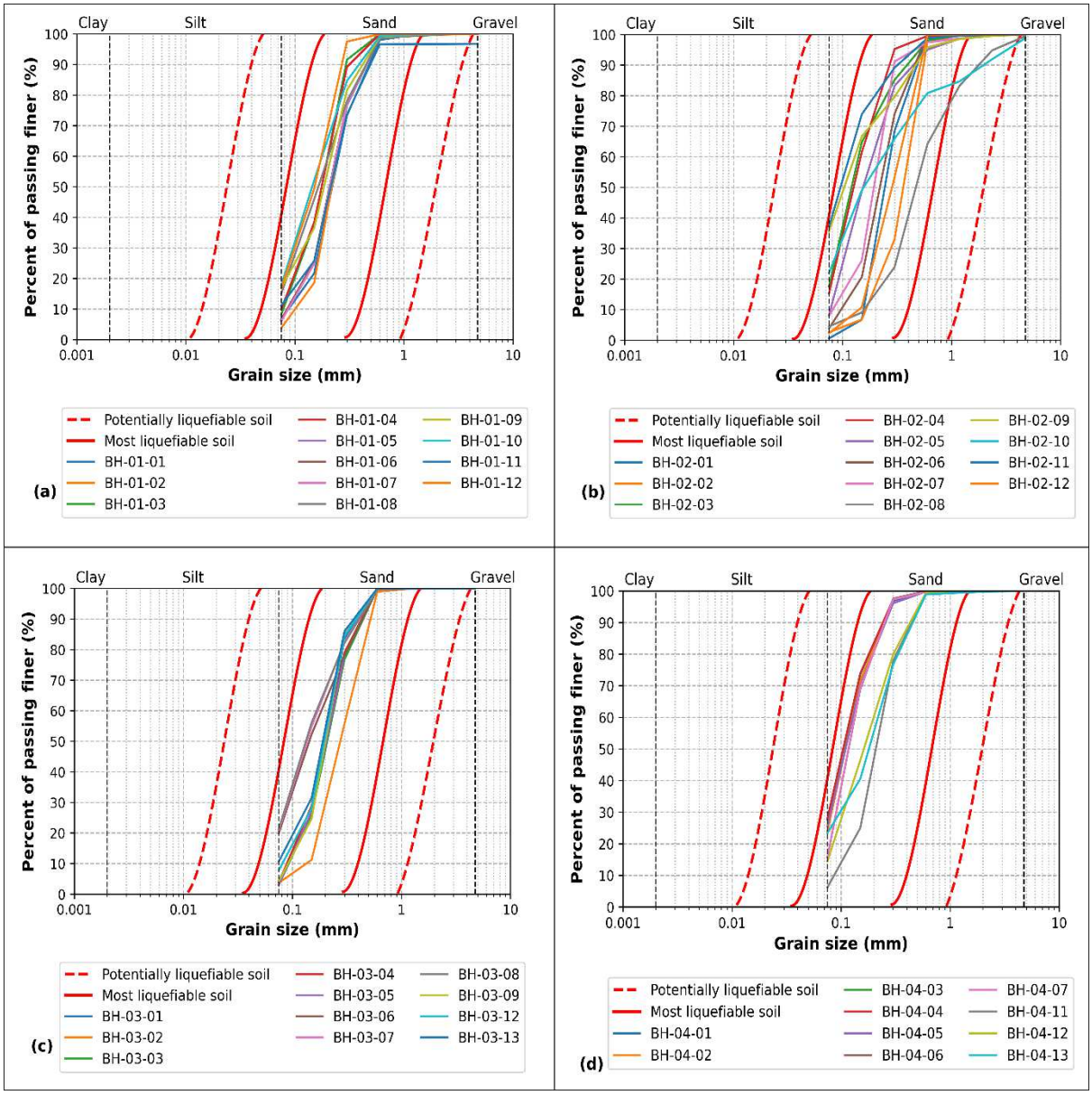

Fig. 5 Grain-size distribution curves of cohesionless soil samples from (a) BH-01, (b) BH-02, (c) BH-03, and (d) BH-04 plotted on the liquefaction susceptibility criteria curves of Iwasaki [51]

The groundwater table was recorded at shallow depths ranging from 0.10 m at BH-02 to 2.74 m at BH-03, shallowing toward the shoreline and deepening northward, near the topographically higher, hilly margin of the island. Table 2 presents the groundwater table depths measured at each borehole with borehole information.

Table 2. Groundwater table depth of all four boreholes from the ground surface

Borehole ID	Coordinates		Groundwater table depth (m)	Drilling Depth (m)
	Latitude (N)	Longitude (E)		
BH-01	21°31'18.10"N	91°55'13.30"E	0.25	19.5
BH-02	21°31'15.90"N	91°54'23.80"E	0.10	19.5
BH-03	21°32'49.40"N	91°55'27.70"E	2.74	19.5
BH-04	21°32'8.30"N	91°55'39.90"E	0.40	19.5

Table 3. Summary of index geotechnical properties of representative soil samples from boreholes BH-01 to BH-04, including moisture content, specific gravity, bulk unit weight, grain size distribution, Atterberg limits, and USCS soil classification

Borehole ID	Sampling Depth (m)	Moisture Content (%)	Specific Gravity	Bulk Unit Weight (kN/m^3)	Grain Size Analysis		Atterberg Limit Tests			Soil Classification (USCS)
					Sand (%)	Fines (%)	LL (%)	PL (%)	PI (%)	
BH-01	1.5	20.02	2.65	20.38	93.31	6.69		Non-Plastic		SP-SM
	3	14.41	2.65	21.52	96.21	3.79		Non-Plastic		SP
	4.5	20.95	2.63	20.11	91.76	8.24		Non-Plastic		SP-SM
	6	22.23	2.64	19.94	90.15	9.85		Non-Plastic		SP-SM
	7.5	20.37	2.63	20.22	93.81	6.19		Non-Plastic		SP-SM
	19.5	33.68	2.63	18.28	1.75	98.25	37.52	18.86	18.66	CL
BH-02	1.5	22.63	2.65	19.92	99.42	0.58		Non-Plastic		SP
	3	20.61	2.63	20.17	97.43	2.57		Non-Plastic		SP
	4.5	23.79	2.64	19.96	82.35	17.65		Non-Plastic		SM
	6	25.28	2.65	19.50	84.69	15.31		Non-Plastic		SM
	7.5	23.20	2.63	19.73	91.82	8.18		Non-Plastic		SP-SM
	19.5	28.40	2.63	18.96	4.52	95.48	30.64	22.30	8.33	CL
BH-03	7.5	17.78	2.62	20.65	96.89	3.11		Non-Plastic		SP
	13.5	47.12	2.66	17.03	2.02	97.98	51.43	25.88	25.55	CH
	15	51.74	2.64	16.61	3.22	96.78	49.45	28.11	21.34	ML
	16.5	22.00	2.63	19.93	92.20	7.80		Non-Plastic		SP-SM
	18	22.50	2.65	19.94	89.32	10.68		Non-Plastic		SP-SM
BH-04	10.5	25.46	2.64	19.43	84.11	15.89		Non-Plastic		SM
	12	29.89	2.68	18.96	38.71	61.29	26.86	14.99	13.87	CL (Sandy)
	13.5	26.53	2.67	19.39	44.26	55.74	23.85	13.97	9.88	CL (Sandy)
	15	19.64	2.68	20.60	48.58	51.42	23.39	14.50	8.88	CL (Sandy)
	16.5	19.82	2.65	20.42	84.05	15.95		Non-Plastic		SM

5.2 Liquefaction Susceptibility of Fine-Grained Soil

Based on the Bray and Sancio [34] criteria, the fat clay (CH) and silt (ML) layers in BH-03 (13.5–15.0 m) and the lean clay (CL) at the base of BH-01 (19.5 m) exhibit PI > 18, categorizing them as not susceptible to liquefaction (Fig. 6). These layers were designated as non-liquefiable zones throughout the study. In contrast, the sandy lean clay (CL) samples from BH-04 (13.5–15.0 m) and the lean clay (CL) sample from BH-02 (19.5 m) plot within the susceptible domains due to low plasticity (PI = 8.33% to 13.87%) and elevated in-situ moisture ratios (Wc/LL > 0.85) (Figure 6). Only the sandy lean clay sample from BH-04 at 12 m depth is identified as moderately susceptible, which requires further laboratory investigation.

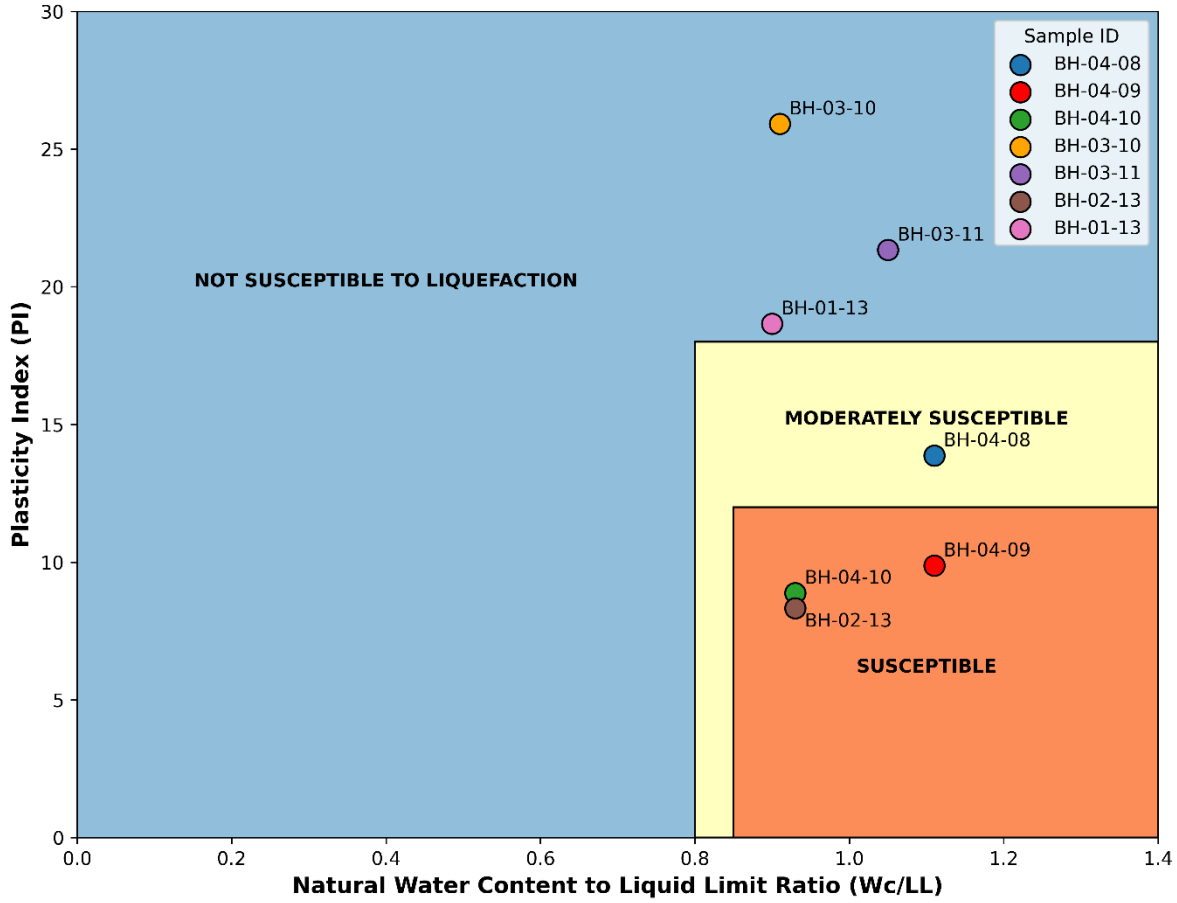

Fig. 6 Liquefaction susceptibility assessment of fine-grained soil samples based on the Bray and Sancio [34] criteria

5.3 Factor of Safety (F.S.) Against Liquefaction

Depth profiles of CSR, CRR, and factor of safety for all four boreholes under different earthquake-magnitude scenarios at a peak ground acceleration of 0.28 g show pronounced stratigraphic and magnitude-dependent triggering responses (Figure 7). Table 4 represents an example of calculations of factor-of-safety for Borehole 2 using the software. Values displayed as 5.0 represent the software's upper reporting limit, where applicable, and should not be interpreted as exact factor-of-safety values unless confirmed by the underlying calculation output.

At the historical earthquake magnitude of 5.2, BH-02 exhibits the most variable liquefaction response, with the 4.5 m, 7.5 m, and 10.5 m depth layers falling below the F.S. threshold, and the minimum F.S. value reaching 0.64,

indicating liquefaction triggering (Figure 7a). The recurrence of F.S. below the threshold in those layers indicates that the CSR consistently exceeds the CRR, pointing to isolated loose sandy layers in the borehole, even under relatively modest seismic loading. BH-01 and BH-04 exhibit the highest liquefaction resistance, with all investigated layers having F.S. values greater than 1. BH-03 shows only one liquefiable layer at a depth of 18.0 m (F.S. = 0.77), indicating very low liquefaction susceptibility (Figure 7a). Overall, most subsurface layers across the area remain stable.

In the case of a magnitude 6 earthquake, liquefiable layers extend significantly compared to the historical earthquake magnitude. BH-02 continuously records F.S. values less than 1 at depths of 1.5 to 12 m, except for the 3 m and 6 m depth layers. BH-01 remains comparatively stable, with only liquefiable layers occurring within the upper 3 m of the profile. In BH-03, liquefiable layers are identified at depths of 3.0 m, 18.0 m, and 19.5 m, indicating the development of both shallow and deep liquefied zones. BH-04 shows liquefiable layers up to 3 m depth and from 12 m to 18 m depth, except at 15 m depth (Figure 7b).

The CSR value increases substantially, and the factor of safety (F.S.) falls below the threshold limit over a largely continuous depth interval under the M_w = 7.0 earthquake scenario. In BH-02, nearly all layers up to 12 m have F.S. values below 1.0, with a minimum of 0.30. The layer at a depth of 3 m is the only exception. BH-04 shows that layers below 16.5 m depth are fully liquefiable, as are the upper layers up to 4.5 m depth. BH-03 shows the same layered pattern as BH-04, with a continuous susceptible zone between 3.0 and 7.5 m depth, as well as deeper liquefiable layers at 18.0 and 19.5 m. BH-01 exhibits the lowest liquefiable layers, where only the upper 4.5 m becomes liquefiable.

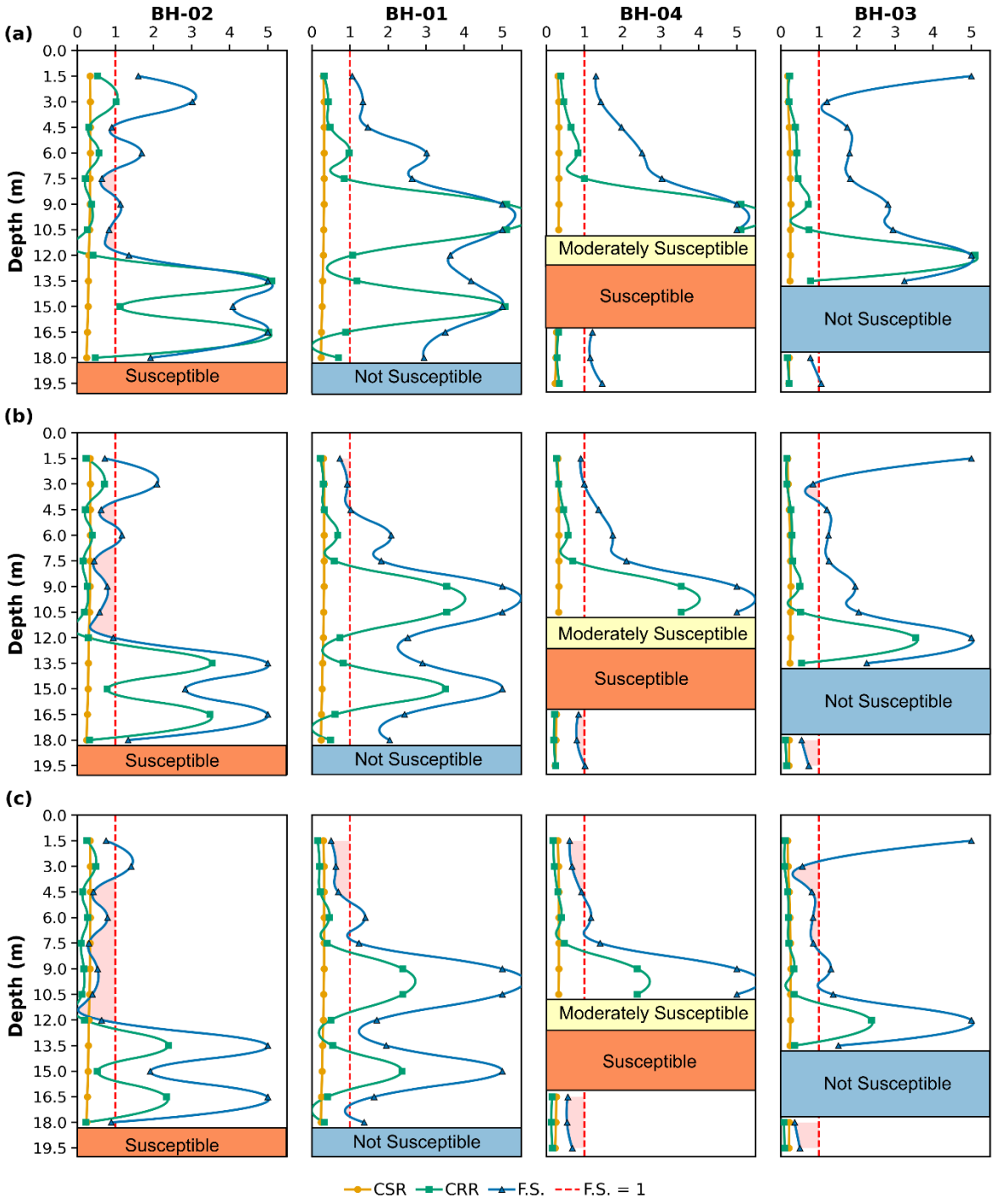

Fig. 7 Depth profiles of Cyclic Stress Ratio (CSR), Cyclic Resistance Ratio (CRR), and Factor of Safety against liquefaction (F.S.) for boreholes BH-01 to BH-04 under three different earthquake magnitude scenarios of M_w = 5.2, 6.0, and 7.0 at a PGA = 0.28 g. Subfigures (a), (b), and (c) represent 5.2, 6.0, and 7.0 magnitude scenarios, respectively. The vertical dashed line (F.S.= 1.0) denotes the liquefaction triggering threshold. The red shaded area represents the liquefied zone

Table 4 Depth wise calculations of cyclic stress ratio (CSR), cyclic resistance ratio (CRR), and factor-of-safety (F.S.) using LiquefyPro software for different earthquake magnitudes at PGA of 0.28 g and groundwater table depth of 0.10 m

Depth (m)	N value	FC (%)	σ_o (kPa)	σ'_o (kPa)	r_d	CSR	C_n	$(N_1)_{60}$	$(N_1)_{60cs}$	CRR			F.S.		
										$M_w = 5.2$	$M_w = 6.0$	$M_w = 7.0$	$M_w = 5.2$	$M_w = 6.0$	$M_w = 7.0$
1.5	16	0.58	29.6	16.2	0.99	0.33	1.70	12.24	12.24	0.53	0.23	0.16	1.6	0.72	0.48
3	34	2.57	59.7	31.5	0.98	0.34	1.70	29.48	29.48	1.02	0.71	0.48	3.02	2.09	1.41
4.5	9	17.65	89.4	46.5	0.97	0.34	1.43	7.33	10.95	0.3	0.21	0.14	0.9	0.62	0.42
6	24	15.31	118.9	61.4	0.95	0.34	1.25	17.05	20.48	0.57	0.39	0.27	1.69	1.17	0.79
7.5	11	8.18	148.6	76.3	0.94	0.33	1.12	7.02	7.45	0.21	0.15	0.1	0.64	0.44	0.3
9	22	3.84	178.1	91.1	0.93	0.33	1.02	13.53	13.53	0.37	0.26	0.17	1.13	0.78	0.53
10.5	16	7.91	207.6	106.0	0.89	0.32	0.95	9.13	9.52	0.26	0.18	0.12	0.83	0.58	0.39
12	28	4.51	237.5	121.1	0.85	0.30	0.89	14.88	14.88	0.41	0.29	0.19	1.35	0.94	0.63
13.5	50	35.55	267.7	136.7	0.81	0.29	0.83	24.93	34.92	5.11	3.54	2.39	5	5	5
15	50	22.04	298.6	152.8	0.77	0.27	0.79	23.60	29.74	1.12	0.78	0.52	4.08	2.83	1.91
16.5	51	37.14	330.4	170.0	0.73	0.26	0.75	22.91	32.49	5.02	3.48	2.34	5	5	5
18	41	2.24	361.8	186.6	0.69	0.24	0.72	17.63	17.63	0.47	0.32	0.22	1.92	1.33	0.89

5.4 Liquefaction Potential Index (LPI)

In this study, LPI values have been calculated from the factor of safety profiles under each earthquake scenario and categorized by following the Iwasaki et al. [21] classification. Figure 8 presents the distribution of LPI values across the four boreholes together with the corresponding liquefaction hazard categories.

Under a 5.2 magnitude scenario, BH-01 and BH-04 recorded an LPI value of 0.00, indicating very low liquefaction potential, whereas BH-03 recorded an LPI value of 0.35, corresponding to the low liquefaction potential category. In contrast, BH-02 recorded an LPI value of 5.75, placing it within the high potential category. With an increase in earthquake magnitude to M_w 6.0, the LPI values increased considerably in all boreholes. BH-02 reached an LPI value of 18.72 and entered the very high potential category. BH-01, BH-03, and BH-04 recorded LPI values of 4.64, 2.83, and 2.24, respectively, indicating low liquefaction potential. Under the M_w 7.0 scenario, liquefaction potential increased markedly across the study area. BH-01 and BH-02 entered the very high potential category with LPI values of 15.26 and 29.59, respectively. BH-03 and BH-04 recorded LPI values of 12.05 and 12.51, respectively, and remained within the high potential category. Among all boreholes, BH-02 consistently exhibited the highest LPI values under all earthquake scenarios.

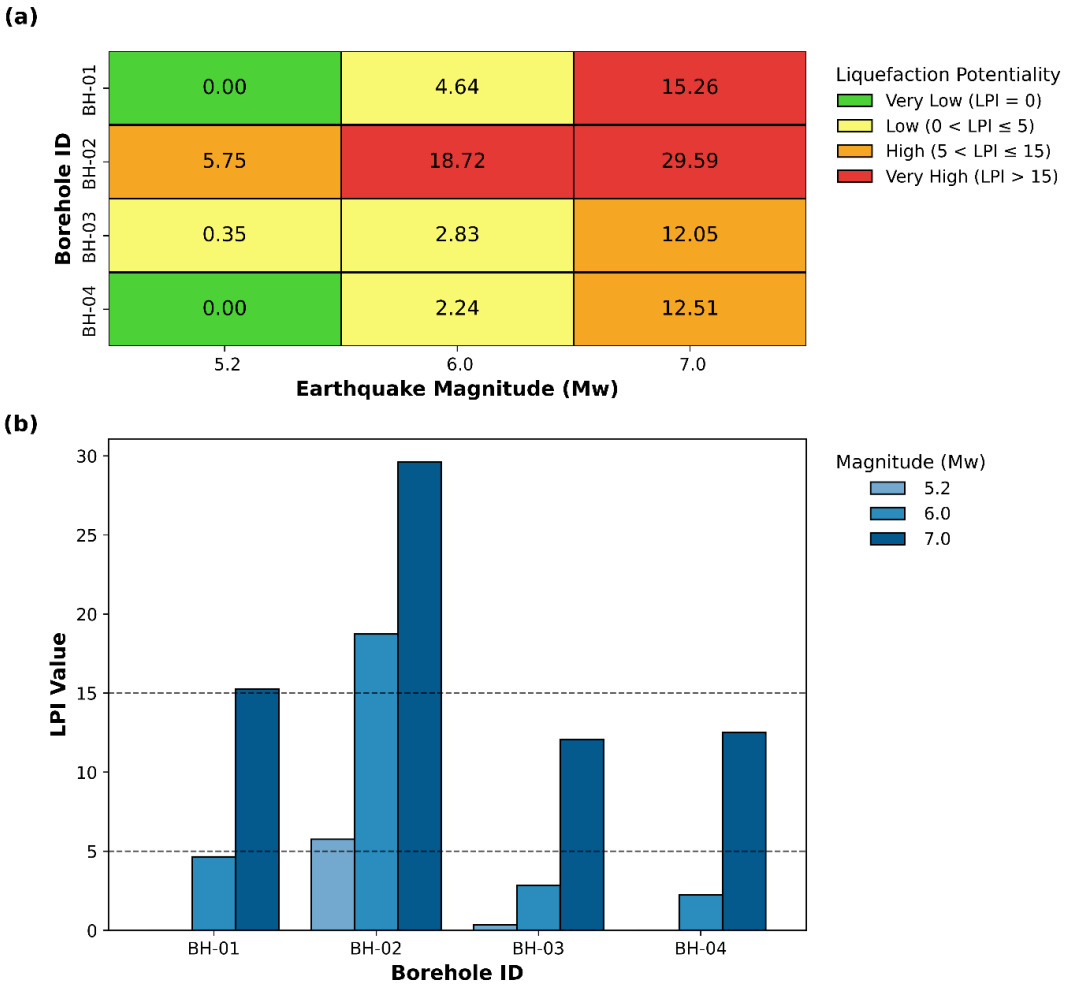

Fig. 8 Liquefaction Potential Index (LPI) values and corresponding potential categories under different earthquake magnitude scenarios. (a) Heatmap matrix showing the spatial variation of LPI values across the four boreholes (BH-01 to BH-04) for earthquake magnitudes of 5.2, 6.0, and 7.0. Color represents liquefaction hazard categories according to the LPI classification. (b) Comparative bar chart illustrating the corresponding LPI values for each borehole under the three earthquake scenarios, with dashed lines indicating the threshold values between different classes

5.5 Post-liquefaction Ground Settlement

The calculated cumulative post-liquefaction settlement represents the estimated free-field vertical volumetric settlement of the soil layers. Cumulative post-liquefaction settlement values increased progressively with earthquake magnitude increment in all boreholes, as illustrated in Figure 9.

At an earthquake magnitude of M_w 5.2, BH-02 recorded the highest total settlement of 10.55 cm, whereas BH-01 and BH-04 recorded approximately zero total settlement (0 cm). BH-03 recorded total settlement of 4.71 cm. Under the M_w 6.0 earthquake scenario, settlement values increased substantially, where BH-02 again exhibited the highest total settlement (24.42 cm), while BH-01, BH-03 and BH-04 recorded total settlements of 6.69 cm, 12.71 cm and 12.05 cm, respectively. The magnitude 7 scenario produced the maximum cumulative settlement across the study area. BH-02 recorded the highest total settlement of 28.87 cm, followed by BH-03 (24.27 cm) and BH-04 (19.92 cm), whereas BH-01 recorded less settlement comparatively, with a total settlement of 9.84 cm. These results indicate differences in the calculated settlement response among the investigated borehole profiles under the adopted magnitude-sensitivity cases.

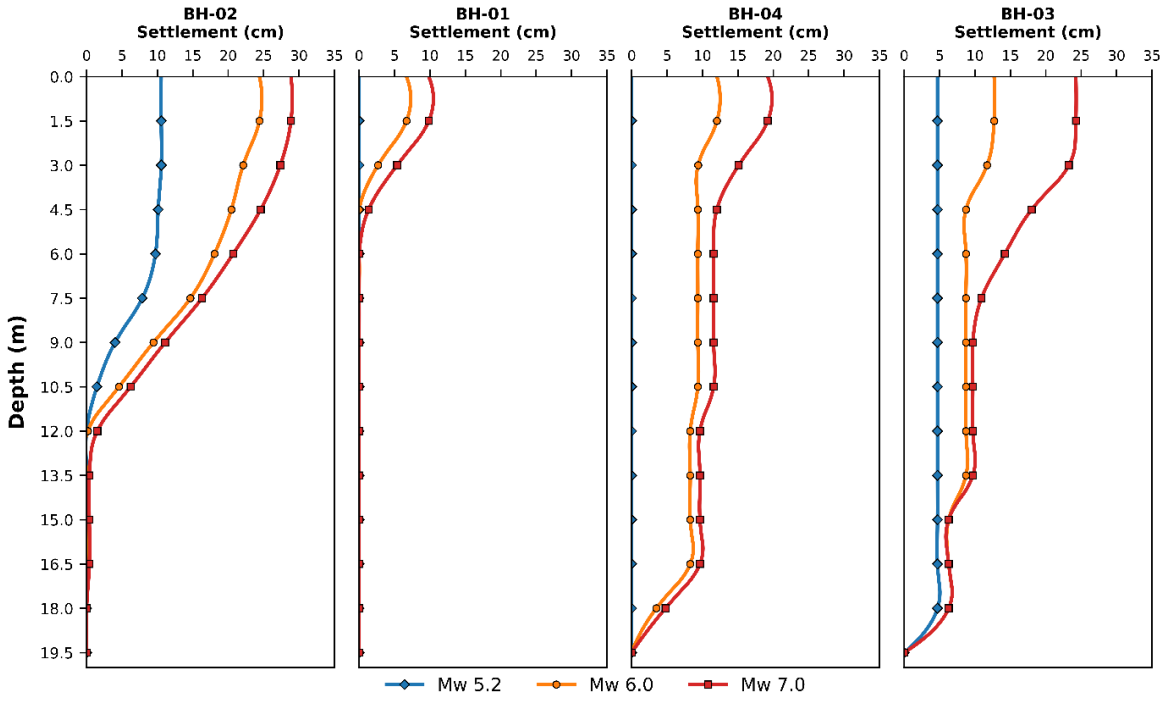

Fig. 9 Depth-wise variation of cumulative post-liquefaction settlement for the four investigated boreholes (BH-01–BH-04) under three earthquake scenarios (M_w = 5.2, M_w = 6.0, and M_w = 7.0 and at PGA of 0.28 g)

6 Discussion

6.1 Liquefaction Potential, Surface Manifestation, and Damage Potential

The LPI results complement the factor-of-safety profiles by providing a cumulative measure of liquefaction severity for each borehole [8, 21, 24]. Liquefaction potential in general increases with increasing earthquake magnitude, but the rate and pattern differ by site. At 5.2 magnitude, BH-02 indicates high liquefaction potential due to interbedded loose to medium dense sand layers while other boreholes sites show very low to low potential. At M_w 6.0 all four boreholes respond, and at M_w 7.0 the response is substantial everywhere. With increasing magnitude scenarios, liquefaction hazard becomes severe and widespread across the study area. BH-01 showed the largest change in hazard class with increasing magnitude. Its LPI more than tripled between M_w 6.0 and 7.0, moving from low to very high potential. This shows that locations that appear safe under moderate shaking can become vulnerable under strong shaking, so a hazard classification based on a single scenario can be misleading. Al-Enezi et al. [22] conducted research in the coastal cities of Kuwait, where liquefaction potential increased systematically with earthquake magnitude, in both severity and areal extent. Several studies in the coastal regions of Bangladesh have also reported high to very high liquefaction hazard potential at different seismic loadings [2, 7, 24].

Liquefaction can damage infrastructures, foundations, and lifelines through liquefaction-induced surface manifestations like sand boils, ground cracking, lateral spreading, and ground subsidence. Toprak and Holzer [52] suggested occurrence of sand boils with LPI > 5 and lateral spreading with LPI > 12. At a magnitude of 7.0 and a PGA of 0.28 g, all sites, which are predominantly underlain by saturated Holocene sandy and silty sand coastal deposits, exceed both LPI thresholds, indicating high to very high liquefaction potential and suggesting an increased likelihood of surface manifestations, such as sand boils and lateral spreading. However, BH-03 (12.05) and BH-04 (12.51) exceed the LPI = 12 threshold only marginally, and BH-01 (15.26) exceeds the very-high boundary of 15 only marginally, so these classifications are near-threshold and should not be over-interpreted. The historical earthquake events also caused lateral spreading, sand boils, and fissures in saturated Holocene sandy and silty soils in different areas of Bangladesh [3]. LPI does not account for the thickness of the non-liquefied surface layers, which controls whether excess pore pressure can breach the crust. Ishihara [36] showed that where the non-liquefiable surface layer (H_1) is thick relative to the liquefiable layer (H_2), the resulting excess pore pressure will not be powerful enough to breach the crust and surface manifestation will not happen. At BH-03, a 1.5 m thick non-liquefiable surface layer overlies a liquefiable layer of 1.5 m and 6 m thickness under the M_w 6.0 and M_w 7.0 earthquake scenarios, respectively, at a PGA of 0.28 g according to the SPT-based analysis. In Ishihara's boundary-curves in Figure 10, the M_w 7.0 case plots well inside the damage zone, to the left of the 0.2 g curve, and the M_w 6.0 case plots on the 0.2 g curve and inside the 0.3 g curve, which is the closest reference to the 0.28 g input. Surface damage is therefore likely at BH-03 in both scenarios, even though the M_w 6.0 LPI (2.83) falls below the threshold of 5 for sand boils [52]. Yilmaz and Yavuzer [23] reported that liquefied layers at greater depths may contribute to ground damage, even when LPI values are low, which is consistent with the 12.71 cm of calculated total settlement and deep liquefied layers of BH-03. Moreover, no non-liquefied surface layer was found from the analysis at the other three sites and surface manifestations are likely to occur at both scenarios. In contrast, BH-02 has a 3 m crust above a 1.5 m liquefiable layer at M_w 5.2. It plots to the

right of the 0.3 g curve (Figure 10), so Ishihara's criterion predicts no ground damage at 0.28 g despite an LPI of 5.75, because the liquefied layers are isolated and deep [52].

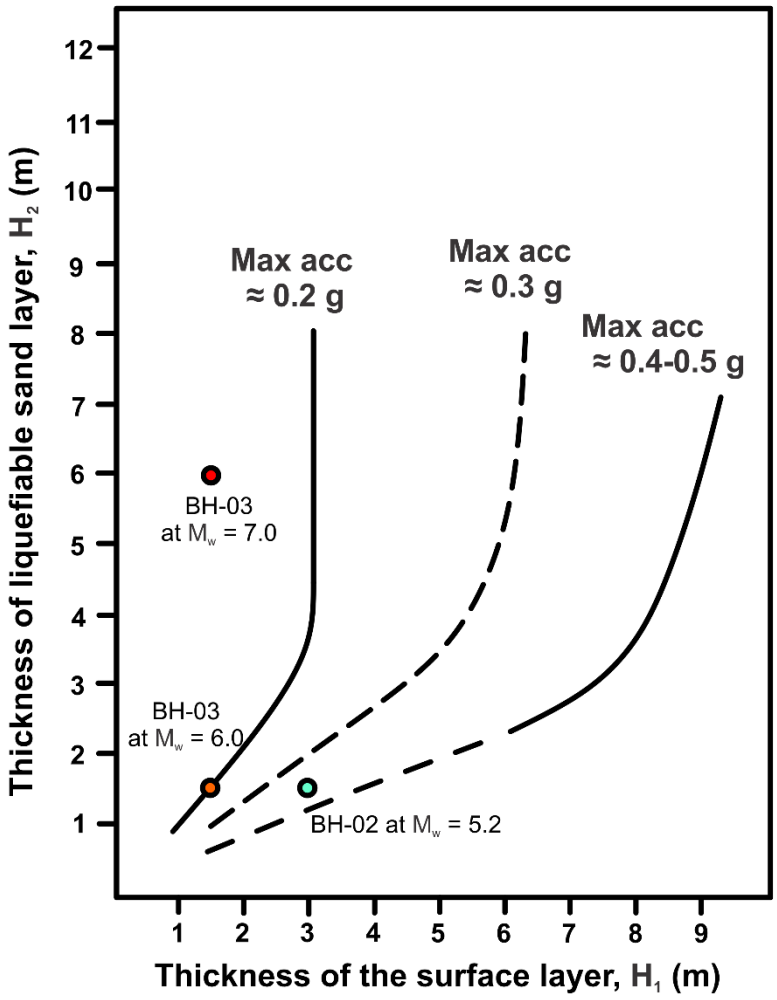

Fig. 10 Assessment of liquefaction-induced ground damage potential using the boundary curves proposed by Ishihara [36]. Under the considered seismic scenarios, BH-03 indicates potential for surface manifestations of liquefaction, whereas BH-02 shows no apparent potential for surface manifestations

The disagreement between the two criteria at BH-02 and BH-03 reflects the different weighting each method gives to depth and thickness, together with the heterogeneity of the subsurface, so both should be used together in site assessment. Post-liquefaction settlement may be more consequential for infrastructure than liquefaction triggering alone [2]. Settlement increases progressively with earthquake magnitude across all boreholes, consistent with increases in liquefiable thickness and reductions in factor of safety. At M_w 7.0 they range from 9.84 cm (BH-01) to 28.87 cm (BH-02), a difference of about 19 cm that could produce differential settlement between adjacent foundations or interconnected structures, depending on separation. Bray et al. [53] reported ground and building settlements of approximately ranging from 10 to 30 cm in the Christchurch Central Business District that experienced significant

structural distortion, differential settlement and in one case demolition, following the 2011 Christchurch earthquake. Overall, the spatial variation of total settlement at the ground surface under the earthquake scenarios can adversely affect any foundations or interconnected overlying structures. But under all scenarios, BH-01 shows the lowest settlements among the boreholes, reaching just 9.84 cm even at magnitude 7.0. This response is consistent with the presence of thick, dense to very dense sandy layers below 4.5 m to 18 m depth, where F.S. remains above 1.0, resulting in a near-zero calculated volumetric strain contribution from this interval [4]. LPI and settlement did not rank the boreholes consistently. At M_w 6.0, BH-01 has about twice the LPI of BH-04 (4.64 vs 2.24) but about half its settlement (6.69 vs 12.05 cm), and BH-03 and BH-04 settle almost twice as much as BH-01 despite lower LPI values. At M_w 7.0, BH-01 has the second-highest LPI (15.26) but the lowest settlement (9.84 cm). These differences arise because LPI weights shallow layers and keeps responding as FS decreases, whereas settlement depends on volumetric strain, which approaches an upper limit once FS is well below 1, and on the thickness of liquefied layers regardless of depth. LPI therefore expresses the severity of shallow liquefaction and settlement the cumulative deformation, and neither alone represents ground-deformation potential. This indicates that LPI alone may not fully represent the magnitude of ground deformation and surface manifestation potential in such heterogeneous subsurface condition.

6.2 Geological and Geotechnical Controls on Liquefaction Potential

The geomorphological and geotechnical characteristics (Sect. 2 and 5.1) of the area indicate Holocene coastal deposits (alternation of sand, silt, and clay), which are highly susceptible to liquefaction according to the ground failure susceptibility criteria of Youd and Perkins [54]. The low-lying coastal position and regional seismicity associated with active tectonics also indicates the area's high susceptibility to earthquake-induced liquefaction [23]. The poorly graded sandy soils fall within the range of most liquefaction susceptibility of Iwasaki [51] gradation curve criteria. The combination of loose, saturated sandy soils and a shallow groundwater table satisfies the fundamental criteria for earthquake-induced liquefaction susceptibility across the study area [1, 12]. The results indicate that liquefaction potential varies spatially across the study area and is strongly influenced by site-specific geotechnical conditions, including grain-size distribution, relative density as reflected by SPT N-values, fine content (%), plasticity characteristics, and groundwater conditions. Rather than treating the observed spatial variability as an unexplained artifact, this variability can be interpreted as a direct geotechnical expression of the open to semi-protected depositional system of the western young coastal plain of the island, documented by Majlis et al. [32]. The sandy soils are poorly graded, and their deposition and distribution are dominated by Holocene sea-level changes, monsoon climate, tides, waves, and high-energy conditions. The clay-rich layers interbedded with sandy deposits are possibly deposited in a back-barrier lagoonal environment [32]. Stratigraphic heterogeneity directly governs the vertical distribution of factor-of-safety values across the investigated profiles (Fig. 4, Fig. 7). Moreover, the location of boreholes within the setting also controls the liquefaction potential along with the variation of geotechnical properties. For example, BH-02 is located near the coast, within the transitional zone between the intertidal and supratidal environments. The subsurface consists of complex alternations of sandy strata with variable SPT N-values and fines contents, and the site has the shallowest groundwater table among the investigated locations. This site exhibits pronounced variation in liquefaction response (high liquefaction potential even at 5.2 magnitude scenario) and surface manifestation potential at different scenarios considered. The importance of saturation for liquefaction is also evidenced in this study by BH-03, where a

loose sandy layer at a depth of 1.5 m remains non-liquefiable under all earthquake scenarios. Rahman and Siddiqua [7] also reported that Holocene sandy and silty soils are non-liquefiable when they remain above the groundwater table. Overall, the shallow groundwater table encountered during field investigation is consistent with high liquefaction susceptibility in the area.

The fine-grained soils present in all the boreholes also exhibit varying liquefaction susceptibility under the Bray and Sancio [34] criteria. Fine-grained soils of BH-04 at different depths exhibit different liquefaction susceptibility. The soil layer at 12 m depth is moderately susceptible, while layers below 12 m and up to 15 m depth are highly susceptible due to variation in plasticity characteristics and moisture content. This can be attributed to lithologic complexity and plasticity variations resulting from variations in depositional conditions that directly influence liquefaction. According to Boulanger and Idriss [55], soils with PI > 7 may exhibit clay-like behavior and may undergo cyclic softening rather than classic sand-like liquefaction to cause significant shear strains and strength loss during seismic loading. The non-susceptible high plasticity layers of BH-03 at 13.5 and 15 m depth may also exhibit clay-like behavior and undergo cyclic softening. Cho et al. [18] documented significant building settlements in a coastal city (Pohang) of South Korea during an intermediate earthquake event (M_w < 6.0) and in the complete absence of surface manifestations like sand boils, which was attributed to the cyclic softening of high-plasticity silt and clay layers (with PI ranging from 25.8% to 28.7%) that are also classified as non-susceptible under the Bray and Sancio [34] criteria. The substantial spatial and depth-wise variation in geotechnical properties due to the heterogeneous depositional environment with varying energy conditions and reworking processes makes liquefaction assessment complex in such an environment. Despite their close proximity, no two boreholes show nearly similar liquefaction response under a unique seismic loading. This indicates that liquefaction susceptibility across the study area is not randomly distributed but is likely governed by depositional processes, specifically, tidal and wave energy variation, back-barrier lagoonal processes, and the resulting alternation of sandy and clay-rich units.

6.3 Implications for Coastal Infrastructure

The liquefaction hazard assessment in this study revealed liquefiable sandy soils at shallow depths under a moderate earthquake scenario of Mw = 6.0 and PGA = 0.28 g, which are prone to ground damage. The shallow foundations of any structures will be affected, causing significant damage. Ground improvement is necessary before any construction when a shallow foundation is required and cannot bypass the shallow, relatively loose, liquefiable layers [2, 7]. Different techniques like densification or solidification, vibro-compaction, or compaction grouting can be useful for liquefaction hazard mitigation. Misliniyati et al. [17] suggested that soil solidification is the most effective mitigation strategy in similar setting. The lowering of groundwater level through drainage is also useful for minimizing risk [23]. The improvement techniques should be used depending on the depth of occurrence of liquefied layers. A notable finding from this study is the identification of relatively dense to very dense layers, mostly composed of silty sand (SM), with raw SPT N values greater than 30 that generally do not liquefy even under a strong earthquake scenario (Figure 11). These layers generally maintain F.S. > 1.0 across all magnitude scenarios considered. These layers can be suggested as a potential zone for deep foundations for the government's heavy infrastructure planning due to relatively high SPT N values and non-liquefiable nature [2]. However, the continuity, bearing capacity, and settlement

behavior of these layers have not been established by the present dataset. Site-specific pile load testing to determine the bearing capacity and foundation settlement should be evaluated before it is used for infrastructure development. The thickness and occurrence of these non-liquefied layers vary across the boreholes. They occur at about 6–12 m at BH-01, BH-03, and BH-04, and at 13.5–16.5 m at BH-02, where the 18 m layer liquefies at M_w 7.0. They are thick and continuous at BH-01 (about 6–18 m), but thinner and interrupted by softer or liquefiable layers elsewhere. At BH-04, for example, the dense sand at 7.5–10.5 m is underlain by susceptible fine-grained soils and liquefiable sand, so it cannot be relied on as a bearing layer without deeper investigation. Foundations at these sites must be designed for liquefaction-induced downdrag and loss of lateral support.

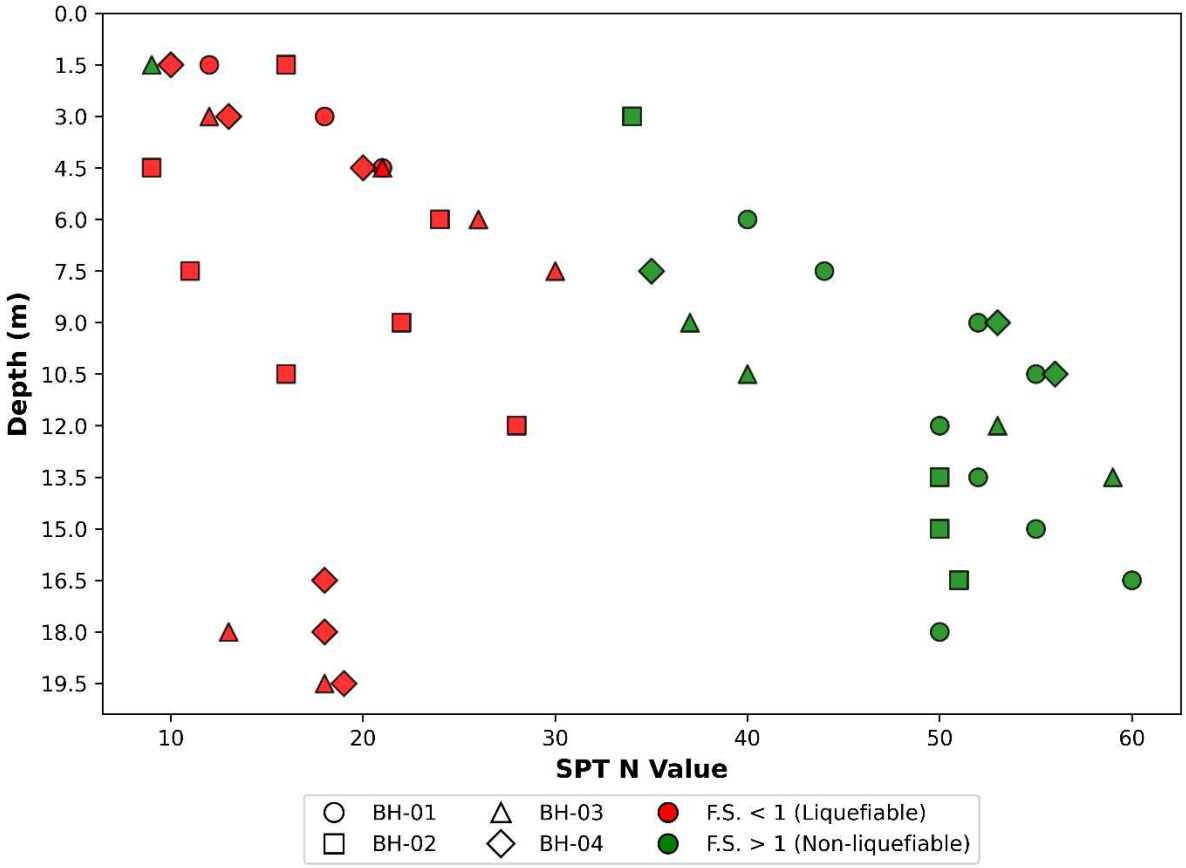

Fig. 11 Depth-wise distribution of liquefiable and non-liquefiable soils based on SPT N-values across the four boreholes for an earthquake magnitude of Mw 7.0 and a peak ground acceleration (PGA) of 0.28 g. Under this maximum considered seismic scenario, soil layers with SPT N-values greater than 30 generally exhibit non-liquefiable behavior

6.4 Limitations of the Study

Despite the valuable insights, this study has some limitations. Firstly, the analysis is based on four boreholes drilled in the protected supratidal deposits, which may not fully represent lateral heterogeneity and continuity of competent layers across the broader coastal plain. Additionally, the use of a deterministic framework with fixed PGA (0.28 g)

represents a generalized approach with magnitude sensitivity assessment and does not account for site-specific ground motion. Moreover, GWL data were collected during the late monsoon season, and temporal variations outside of this period could impact the assessment, which has not been addressed. Finally, the liquefaction susceptibility behavior of fine-grained soils remains difficult to characterize without cyclic triaxial testing and clay-like soils should be assessed for liquefaction resistance using appropriate methods, which is absent in this study. Despite these limitations, the study provides valuable insights into liquefaction hazard in Holocene coastal deposits of the island.

7 Conclusion

This study presents a site-specific liquefaction hazard assessment for coastal infrastructure development on the Holocene coastal deposits of Moheshkhali Island, Bangladesh by combining earthquake-induced liquefaction triggering, liquefaction potential, post-liquefaction settlement estimation, and fine-grained soil liquefaction susceptibility assessment under three earthquake magnitude scenarios at a fixed peak ground acceleration of 0.28 g. The results reveal substantial variability in calculated liquefaction response among the investigated profiles, consistent with differences in soil stratigraphy, penetration resistance, fines content, plasticity characteristics, and groundwater depth. Alternating cohesionless and cohesive deposits create pronounced differences in liquefaction response and no two sites showed similar responses within a single a surface geologic unit, highlighting the necessity of site-specific geotechnical investigations and liquefaction assessment in such complex coastal depositional environments. The key findings from this study are as follows:

1. The investigated profiles consist of alternating sandy, silty, and clay-rich deposits with variable SPT N-values and fines content. Shallow groundwater and loose sandy and silty sand layers contribute to the calculated liquefaction susceptibility of the investigated locations. The fine-grained soils show variable response to liquefaction susceptibility depending on the water content and plasticity behavior. High-plasticity fine-grained soils are generally resistant to classical sand-like liquefaction but may undergo cyclic softening.
2. The combined evaluation of factor of safety (F.S.), Liquefaction Potential Index (LPI), and post-liquefaction settlement consistently shows that liquefaction severity and associated ground deformation potential increase with increasing adopted earthquake magnitude under the fixed-PGA sensitivity scenarios across all boreholes. BH-02 ranks highest by LPI (5.75, 18.72 and 29.59) and by settlement (10.55, 24.42 and 28.87 cm) at M_w 5.2, 6.0 and 7.0, because of its shallow water table and loose interbedded sands, although Ishihara's criterion predicts no surface damage there at M_w 5.2. Overall LPI, settlement, and Ishihara's crust-thickness criterion did not rank the sites consistently: LPI emphasizes shallow layers, settlement reflects the total thickness of liquefied soil, and the Ishihara criterion reflects the protective surface crust. In interlayered coastal deposits, these measures should be used together rather than relying on LPI alone.
3. The variability in estimated ground settlement between the boreholes indicates a high spatially varying potential for liquefaction-induced ground deformation at the investigated sites. This may cause significant damage to foundations and interconnected structures, which is critical for infrastructure planning. Surface manifestations are more likely where LPI is high and the crust is thin or absent. Overall, the investigated sites

show high potential for surface manifestations like sand boils, ground cracking, and lateral spreading under seismic loading that can cause damage to any built infrastructure.

4. Relatively dense silty sand (raw N > 30) remained non-liquefiable in nearly all cases (BH-02 at 18 m under Mw 7.0 being the exception), as expected from the bounded SPT-based CRR curve, and may be a potential bearing stratum for piles, although its lateral continuity, bearing capacity, and settlement must be confirmed by additional borings and pile load tests.

This study makes a meaningful contribution by linking borehole-scale stratigraphy, magnitude-based seismic loading, and three complementary liquefaction indicators into a single interpretation. Moreover, the study also suggests ground improvement techniques like soil densification and improvement of drainage for liquefiable layers to withstand the liquefaction hazard. Therefore, the results of this study are important for coastal development and earthquake-resilient infrastructure planning for safe and sustainable execution of the projects. Incorporating fine-grained soil susceptibility, site-specific liquefaction triggering, LPI-based classification, and liquefaction-induced settlement analysis provides a coherent picture of spatially and vertically variable hazard and therefore offers a useful framework for sustainable and site-specific foundation engineering practice that may be adapted to other active coastal areas of the Bengal Basin and analogous coastal environments.

References

1. Seed, H.B., Idriss, I.M.: Simplified Procedure for Evaluating Soil Liquefaction Potential. J. Soil Mech. Found. Div. 97, 1249–1273 (1971). https://doi.org/10.1061/JSFEAQ.0001662

2. Hossain, A.T.M.S., Mahabub, M.S., Dutta, T., Khatun, M., Terao, T., Imam, M.H., Sayem, H.M., Haque, M.E., Khan, P.A., Jafrin, S.J.: The Hidden Earthquake Induced Liquefaction Risks in the Rohingya Refugee Camp Hills & Surrounding Areas of Ukhiya, Cox’s Bazar, Bangladesh—A Geotechnical Engineering Approach. Open J. Earthq. Res. 12, 114–138 (2023). https://doi.org/10.4236/ojer.2023.123004

3. Jui, T.J., Hossain, M.S., Kamal, A.S.M.M., Rahman, M.Z., Sahebi, M.T., Hossain, A.: Paleoliquefaction mapping for Bangladesh from the records of historical earthquakes. Bull. Eng. Geol. Environ. 84, 291 (2025). https://doi.org/10.1007/s10064-025-04316-w

4. Ishihara, K., Yoshimine, M.: Evaluation of Settlements in Sand Deposits Following Liquefaction During Earthquakes. Soils Found. 32, 173–188 (1992). https://doi.org/10.3208/sandf1972.32.173

5. Iwasaki, T., Arakawa, T., Tokida, K.-I.: Simplified procedures for assessing soil liquefaction during earthquakes. Int. J. Soil Dyn. Earthq. Eng. 3, 49–58 (1984). https://doi.org/10.1016/0261-7277(84)90027-5

6. Boulanger, R.W., Mejia, L.H., Idriss, I.M.: Liquefaction at Moss Landing during Loma Prieta Earthquake. J. Geotech. Geoenvironmental Eng. 123, 453–467 (1997). https://doi.org/10.1061/(ASCE)1090-0241(1997)123:5(453)

7. Rahman, M.Z., Siddiqua, S.: Evaluation of liquefaction-resistance of soils using standard penetration test,

cone penetration test, and shear-wave velocity data for Dhaka, Chittagong, and Sylhet cities in Bangladesh. Environ. Earth Sci. 76, 207 (2017). https://doi.org/10.1007/s12665-017-6533-9

8. Hossain, M.S., Kamal, A.S.M.M., Rahman, M.Z., Farazi, A.H., Mondal, D.R., Mahmud, T., Ferdous, N.: Assessment of soil liquefaction potential: a case study for Moulvibazar town, Sylhet, Bangladesh. SN Appl. Sci. 2, 1–12 (2020). https://doi.org/10.1007/s42452-020-2582-x

9. Idriss, I.M., Boulanger, R.W.: Semi-empirical procedures for evaluating liquefaction potential during earthquakes. Soil Dyn. Earthq. Eng. 26, 115–130 (2006). https://doi.org/10.1016/j.soildyn.2004.11.023

10. Seed, H.B., Idriss, I.M., Arango, I.: Evaluation of Liquefaction Potential Using Field Performance Data. J. Geotech. Eng. 109, 458–482 (1983). https://doi.org/10.1061/(ASCE)0733-9410(1983)109:3(458)

11. Idriss, I.., Boulanger, R..: Soil Liquefcation During Earthquakes. Univ. Calif. Berkeley. 48, (2008)

12. Youd, T.L., Idriss, I.M., Andrus, R.D., Arango, I., Castro, G., Christian, J.T., Dobry, R., Finn, W.D.L., Harder, L.F., Hynes, M.E., Ishihara, K., Koester, J.P., Liao, S.S.C., Marcuson, W.F., Martin, G.R., Mitchell, J.K., Moriwaki, Y., Power, M.S., Robertson, P.K., Seed, R.B., Stokoe, K.H.: Liquefaction Resistance of Soils: Summary Report from the 1996 NCEER and 1998 NCEER/NSF Workshops on Evaluation of Liquefaction Resistance of Soils. J. Geotech. Geoenvironmental Eng. 127, 817–833 (2001). https://doi.org/10.1061/(ASCE)1090-0241(2001)127:10(817)

13. Seed, B.H., Tokimatsu, K., Harder, L.F., Chung, R.M.: Influence of SPT Procedures in Soil Liquefaction Resistance Evaluations. J. Geotech. Eng. 111, 1425–1445 (1985). https://doi.org/10.1061/(ASCE)0733-9410(1985)111:12(1425)

14. Ahmad, M., Tang, X.-W., Ahmad, F., Jamal, A.: Assessment of Soil Liquefaction Potential in Kamra, Pakistan. Sustainability. 10, 4223 (2018). https://doi.org/10.3390/su10114223

15. Ansary, M.A., Arefin, M.R., Hore, R.: Development of liquefaction potential map of Dhaka city using SPT test. J. Civ. Eng. 46, 127–140 (2018)

16. Seo, M.-W., Olson, S.M., Sun, C.-G., Oh, M.-H.: Evaluation of Liquefaction Potential Index Along Western Coast of South Korea Using SPT and CPT. Mar. Georesources Geotechnol. 30, 234–260 (2012). https://doi.org/10.1080/1064119X.2011.614322

17. Misliniyati, R., Zalbuin, L., Refrizon, M., Dwi, W., Zhehan, P., Annisa, F.: Liquefaction Risk Assessment and Microzonation in Bengkulu Port Area After a Megathrust Earthquake. Geotech. Geol. Eng. 43, 1–30 (2025). https://doi.org/10.1007/s10706-025-03090-6

18. Cho, Y., Han, J.T., Choo, Y.W., Lee, J., Kim, J., Kim, K., Park, K., Kim, J., Park, H., Kwak, D., Park, D., Asce, A.M., Choi, J.: Assessments of Liquefaction Triggering Using In Situ and Laboratory Tests in Pohang , South Korea. J. Geotech. Geoenvironmental Eng. 150, 1–17 (2024).

https://doi.org/10.1061/JGGEFK.GTENG-12135

19. Rahman, M.Z., Siddiqua, S., Kamal, A.S.M.M.: Liquefaction hazard mapping by liquefaction potential index for Dhaka City, Bangladesh. Eng. Geol. 188, 137–147 (2015). https://doi.org/10.1016/j.enggeo.2015.01.012

20. Sonmez, H.: Modification of the liquefaction potential index and liquefaction susceptibility mapping for a liquefaction-prone area (Inegol,Turkey). Environ. Geol. 44, 862–871 (2003). https://doi.org/10.1007/s00254-003-0831-0

21. Iwasaki, T., Tokida, K.I.., Tatsuoka, F., Watanabe, S., Yasuda, S., Sato, H.: Microzonation for soil liquefaction potential using simplified methods. In: Proceedings of the 3rd International Conference on Microzonation. pp. 1310–1330. , Seattle (1982)

22. Al-Enezi, D., Abdullah, W., Kamal, H.: Assessing Soil Liquefaction Potential for Urban Cities of Kuwait. Geotech. Geol. Eng. 42, 7771–7789 (2024). https://doi.org/10.1007/s10706-024-02950-x

23. Yılmaz, I., Yavuzer, D.: Liquefaction potential and susceptibility mapping in the city of Yalova, Turkey. Environ. Geol. 47, 175–184 (2005). https://doi.org/10.1007/s00254-004-1141-x

24. Kamal, A.M., Sahebi, M.T., Hossain, M.S., Rahman, M.Z., Fahim, A.K.F.: Liquefaction hazard mapping of the south-central coastal areas of Bangladesh. Nat. Hazards Res. 4, 520–529 (2024). https://doi.org/10.1016/j.nhres.2023.12.016

25. Ansary, M.A., Ansary, M., Ahamed, S.: Liquefaction potential assessment of the DMDP area of Bangladesh using CPT-based methods. Nat. Hazards. 120, 9777–9808 (2024). https://doi.org/10.1007/s11069-024-06586-1

26. Tokimatsu, K., Seed, H.B.: Evaluation of Settlements in Sands Due to Earthquake Shaking. J. Geotech. Eng. 113, 861–878 (1987). https://doi.org/10.1061/(ASCE)0733-9410(1987)113:8(861)

27. Mahabub, M.S., Hossain, A.T.M.S., Pahlowan, E.U.D.: Assessment Of Liquefaction Potential From Sirajganj To Kurigram Area, Bangladesh. IOSR J. Mech. Civ. Eng. (IOSR-JMCE. 17, 31–43 (2020). https://doi.org/10.9790/1684-1701033143

28. Alam, M., Alam, M.M., Curray, J.R., Chowdhury, M.L.R., Gani, M.R.: An overview of the sedimentary geology of the Bengal Basin in relation to the regional tectonic framework and basin-fill history. Sediment. Geol. 155, 179–208 (2003). https://doi.org/10.1016/S0037-0738(02)00180-X

29. Hossain, M.S., Khan, M.S.H., Chowdhury, K.R., Abdullah, R.: Synthesis of the Tectonic and Structural Elements of the Bengal Basin and Its Surroundings. In: Mukherjee, S. (ed.) Tectonics and Structural Geology: Indian Context. pp. 135–218. Springer International Publishing, Cham (2018)

30. Ansary, M.A., Al-Hussaini, T., Sharfuddin, M.: Damage assessment of July 22, 1999 Moheshkhali

Earthquake, Bangladesh. 8th ASCE Spec. Conf. Probabilistic Mech. Struct. Reliab. (2001)

31. BNBC: Bangladesh National Building Code (BNBC) 2020. Minist. Hous. Public Work. 2, 3268–3396 (2020)

32. Majlis, A.B.K., Islam, A., Khasru, H., Ahsan, K.: Protected to Open basin Depositional System: an Appraisal for the Late Quaternary Evolution of the Moheshkhali-Kutubdia Coastal Plain, Bangladesh. Bangladesh J. Geol. 26, 64–77 (2013)

33. Shawon, A.A.: Moheshkhali–Matarbari master plan: Bangladesh's $150bn vision, https://www.dhakatribune.com/bangladesh/390609/ca's-press-wing-mida-to-transform

34. Bray, J.D., Sancio, R.B.: Assessment of the Liquefaction Susceptibility of Fine-Grained Soils. J. Geotech. Geoenvironmental Eng. 132, 1165–1177 (2006). https://doi.org/10.1061/(ASCE)1090-0241(2006)132:9(1165)

35. Maurer, B.W., Green, R.A., Cubrinovski, M., Bradley, B.A.: Evaluation of the Liquefaction Potential Index for Assessing Liquefaction Hazard in Christchurch, New Zealand. J. Geotech. Geoenvironmental Eng. 140, 1–11 (2014). https://doi.org/10.1061/(ASCE)GT.1943-5606.0001117

36. Ishihara, K.: Stability of natural deposits during earthquakes. In: 11th International Conference on Soil Mechanics and Foundation Engineering. pp. 321–376. Balkema, San Francisco, USA (1985)

37. Holzer, T.L., Noce, T.E., Bennett, M.J.: Liquefaction Probability Curves for Surficial Geologic Deposits. Environ. Eng. Geosci. 17, 1–21 (2011). https://doi.org/10.2113/gseegeosci.17.1.1

38. Islam, M.K., Hasan, M., Rahman, M., Fayyaz, R., Chowdhury, M., Hamid, T.: Shoreline Dynamics Assessment of Moheshkhali Island of Bangladesh using Integrated GIS-DSAS Techniques. Dhaka Univ. J. Earth Environ. Sci. 11, 1–14 (2023). https://doi.org/10.3329/dujees.v11i1.63707

39. Maitra, M.K., Baquee, A., Majlis, K., Murshed, S., Rahman, S.: Spatial Changes of Land Use / Land Cover of Moheshkhali Island , Bangladesh : A Fact Finding Approach by Remote Sensing Analysis. Dhaka Univ. J. Earth Environ. Sci. 2, 43–54 (2012)

40. Sikder, A.M., Alam, M.M.: 2-D modelling of the anticlinal structures and structural development of the eastern fold belt of the Bengal Basin, Bangladesh. Sediment. Geol. 155, 209–226 (2003). https://doi.org/10.1016/S0037-0738(02)00181-1

41. Uddin, A., Lundberg, N.: Miocene sedimentation and subsidence during continent–continent collision, Bengal basin, Bangladesh. Sediment. Geol. 164, 131–146 (2004). https://doi.org/10.1016/j.sedgeo.2003.09.004

42. Steckler, M.S., Akhter, S.H., Seeber, L.: Collision of the Ganges-Brahmaputra Delta with the Burma Arc: Implications for earthquake hazard. Earth Planet. Sci. Lett. 273, 367–378 (2008).

https://doi.org/10.1016/j.epsl.2008.07.009

43. Gani, M.R., Alam, M.M.: Sedimentation and basin-fill history of the Neogene clastic succession exposed in the southeastern fold belt of the Bengal Basin, Bangladesh: a high-resolution sequence stratigraphic approach. Sediment. Geol. 155, 227–270 (2003). https://doi.org/10.1016/S0037-0738(02)00182-3

44. Steckler, M.S., Mondal, D.R., Akhter, S.H., Seeber, L., Feng, L., Gale, J., Hill, E.M., Howe, M.: Locked and loading megathrust linked to active subduction beneath the Indo-Burman Ranges. Nat. Geosci. 9, 615–618 (2016). https://doi.org/10.1038/ngeo2760

45. Wang, Y., Sieh, K., Tun, S.T., Lai, K., Myint, T.: Active tectonics and earthquake potential of the Myanmar region. J. Geophys. Res. Solid Earth. 119, 3767–3822 (2014). https://doi.org/10.1002/2013JB010762

46. CivilTech Software: LiquefyPro: Liquefaction and Settlement Analysis Software Manual. (2021)

47. Bray, J.D., Sancio, R.B., Durgunoglu, T., Onalp, A., Youd, T.L., Stewart, J.P., Seed, R.B., Cetin, O.K., Bol, E., Baturay, M.B., Christensen, C., Karadayilar, T.: Subsurface Characterization at Ground Failure Sites in Adapazari, Turkey. J. Geotech. Geoenvironmental Eng. 130, 673–685 (2004). https://doi.org/10.1061/(ASCE)1090-0241(2004)130:7(673)

48. Liao, S.S.C., Whitman, R. V.: Overburden Correction Factors for SPT in Sand. J. Geotech. Eng. 112, 373–377 (1986). https://doi.org/10.1061/(ASCE)0733-9410(1986)112:3(373)

49. Blake, T.F.: Summary Report of Proceedings of the NCEER Workshop on Evaluation of Liquefaction Resistance of Soils. , Buffalo, NY (1997)

50. Skempton, A.W.: Standard penetration test procedures and the effects in sands of overburden pressure, relative density, particle size, ageing and overconsolidation. Géotechnique. 36, 425–447 (1986). https://doi.org/10.1680/geot.1986.36.3.425

51. Iwasaki, T.: Soil liquefaction studies in Japan: state-of-the-art. Soil Dyn. Earthq. Eng. 5, 2–68 (1986). https://doi.org/10.1016/0267-7261(86)90024-2

52. Toprak, S., Holzer, T.L.: Liquefaction Potential Index: Field Assessment. J. Geotech. Geoenvironmental Eng. 129, 315–322 (2003). https://doi.org/10.1061/(ASCE)1090-0241(2003)129:4(315)

53. Bray, J., Cubrinovski, M., Zupan, J., Taylor, M.: Liquefaction Effects on Buildings in the Central Business District of Christchurch. Earthq. Spectra. 30, 85–109 (2014). https://doi.org/https://doi.org/10.1193/022113EQS043M

54. Youd, T.L., Perkins, D.M.: Mapping Liquefaction-Induced Ground Failure Potential. J. Geotech. Eng. Div. 104, 433–446 (1978). https://doi.org/10.1061/AJGEB6.0000612

55. Boulanger, R.W.., Idriss, I.M.: Liquefaction Susceptibility Criteria for Silts and Clays. J. Geotech.

Geoenvironmental Eng. 132, 1413–1426 (2006). https://doi.org/10.1061/(ASCE)1090-0241(2006)132:11(1413)